12-1-2015

Effects of stream edges on algal biomass in the middle Rio Grande

Steven Daniel Scholle

Steven Scholle

Candidate

Biology

Department

This thesis is approved, and it is acceptable in quality and form for publication:

Approved by the Thesis Committee:

Thomas Turner , Chairperson

Rebecca Bixby

Robert Sinsabaugh

Grant Meyer

EFFECTS OF STREAM EDGES ON ALGAL BIOMASS IN THE MIDDLE RIO GRANDE

BY

STEVEN D. SCHOLLE

B.S., ENVIRONMENTAL SCIENCE, NEW MEXICO INSTITUTE OF MINING AND TECHNOLOGY, 2008
B.S., BIOLOGY, NEW MEXICO INSTITUTE OF MINING AND TECHNOLOGY, 2008

THESIS

Submitted in Patial Fulfillment of the
Requirements for the Degree of

Master of Science

Biology

The University of New Mexico
Albuquerque, New Mexico

December, 2015

ACKNOWLEDGEMENTS

I thank all those that helped with data collection, particularly: Stacy Scholle, Nathan Lopez-Brody, and Erica Johnson and the rest of the Turner Lab. I thank Chris Castorena and Stacy Scholle for their help with data analysis. I also thank Dr. David Hanson and his lab for assistance with spectrophotometry. Special thanks go to my graduate committee: Drs. Thomas Turner (chair), Rebecca Bixby, Robert Sinsabaugh, and Grant Meyer. Thank you for all your guidance and support! NSF Grant DEB 0717047 funded this work. Lastly, I thank my family and friends for all their love and patience ♡

Contents

List of Figures

List of Tables

EFFECTS OF STREAM EDGES ON ALGAL BIOMASS IN THE MIDDLE RIO GRANDE

by

Steven D. Scholle

B.S., Environmental Science, New Mexico Institute of Mining and Technology, 2008

B.S., Biology, New Mexico Institute of Mining and Technology, 2008

M.S., Biology, University of New Mexico, 2015

ABSTRACT

In river systems, there are many factors that impede or facilitate algal standing stock and therefore impact primary production in these environments. I am particularly interested in the influence of edges in riverine systems and how these geomorphic features affect the available surface area for algal production. This study investigates the middle Rio Grande system near Albuquerque, New Mexico, USA. The middle Rio Grande is a turbid, partially braided lotic ecosystem. Although edge characteristics can vary widely, especially between errosional and depositional banks, I hypothesize that edges become important zones of primary production, due in part to decreased water depth, providing increased light availability. Further, edges may provide regions of lower flow velocity, resulting in reduced substrate turnover and increased nutrient retention, facilitating algal attachment and growth. This study aims to elucidate the relationships among position within a transect (i.e. distance from edge), substrate type (i.e. sand, mud, cobble), water chemistry, turbidity, depth, flow velocity, and algal biomass. I use the analysis of chlorophyll *a* (chl *a*) concentrations as a proxy for algal biomass in samples taken across lateral transects, each with a different predominant benthic substrate. This work develops the understanding of

key contributing abiotic factors that influence primary production in the middle Rio Grande and similar ecosystems by providing insight into the effects of these factors on chl *a* concentrations. Surprisingly, only transects with the sand substrate exhibited my hypothesized pattern of greater primary production near river edges. In contrast, the transects with cobble and mud substrates show the opposite pattern, in which locations far from the river's edge contained the highest algal concentrations. These results highlight the complex interactions of abiotic influences on benthic primary production in these systems.

1 Introduction

Freshwater algae are important components of in-stream primary production in aquatic ecosystems. They provide energy essential to obligate algivores while supporting secondary production important to higher trophic levels (Bunn et al., 2003; Hamilton et al., 2004; Pease et al., 2006). Bunn and Davies (1999) use the term 'bath-tub ring' production to describe algal production in turbid, aridland lotic ecosystems such as the middle Rio Grande, because edge habitat can be particularly important in such ecosystems; increased photosynthetic potential due to light penetration and decreased flow velocities may facilitate benthic attachment and growth of algae in edge habitats (Benda et al., 2004).

In this study I investigate the lateral distribution of in-stream primary production in the middle Rio Grande. The middle Rio Grande is an aridland riverine ecosystem within a ~300-km river reach near Albuquerque, New Mexico. River management practices in the middle Rio Grande have dramatically changed the planform of the reach (Swanson et al., 2011) and may impact algal production by causing changes in depth, velocity, substrate type, and the number of edges, thereby influencing available surface area to support algal growth. A better understanding of the ways that sandbar and island dynamics affect primary production may impact water management practices within the middle Rio Grande. Flynn et al. (2013) discuss the importance of understanding benthic algal dynamics in the context of river management for recreational use (an important economic driver in their region) and such investigations may provide ideas for river management to help support threatened or endangered taxa dependent on algal production including the Rio Grande silvery minnow, *Hybognathus amarus*. This work also contributes to the growing body of research at the interface of fluvial geomorphology and aquatic ecosystem ecology. Geomorphic forms and processes directly influence and are influenced by biological ecosystem components (Swanson et al., 1988). Furthermore, these forms and processes occur at similar

spatial and temporal scales to those studied by ecosystem ecology (Newbold et al., 1982a,b; Junk et al., 1989; Micheli and Kirchner, 2002; Renschler et al., 2007). Thoms and Parsons (2002) and Fisher et al. (2007) discuss the growing interdisciplinary interface between fluvial geomorphology and ecology.

This region of the Rio Grande exhibits high sediment loads and variable flows. I look at some of the relationships between in-stream primary production and fluvial edges, including river edges, bars, and islands. By observing differences in algal standing stock estimated using chl *a* concentrations across three general transect types, I develop linear models exploring the relationships among many characteristics of the system including water chemistry (i.e., pH, temperature, dissolved oxygen), turbidity and light availability, flow characteristics, benthic substrate (i.e., cobble, sand, silt), season, chl *a*, and sampling position within and among transects (i.e., distance from edge of water and water depth). Depth can be particularly important as a major driver of many of the components of the system including light availability, flow velocity, and sediment transport. Comparisons of these various parameters provide important information about the relevance of edges as habitats for algal growth and production. I hypothesize that edges are areas that provide conditions that facilitate the growth of algae and that these areas will display higher primary production as compared to other parts of a given river transect. I am particularly interested in providing a better understanding of the ways that position within the transect (i.e., distance and water depth), substrate type (i.e., silt, sand, or cobble), water chemistry, turbidity, and flow velocity interact with one another and how they affect algal biomass in this system. If edges are important zones of algal growth, then homogenization of a braided channel may reduce instream primary production by reducing the amount of habitat available for algae.

2 Methods

2.1 Study area

Transects for this study are located in two general locations: upstream transects near the US Route 550 Bridge in Bernalillo, New Mexico (with a main-channel transect labelled Bernalillo T2, an island-side-channel transect, Bernalillo T3, and an alternate main-channel transect, Bernalillo T4) and downstream transects near the Alameda Blvd. Bridge in Albuquerque, New Mexico (with a main-channel transect labeled Alameda T1 and an alternate island-side-channel transect labeled Alameda T5). Figures 24, 25, and 26 show photographs of the primary transects used in this study (Alameda T1, Bernalillo T2, and Bernalillo T3) as seen during my late March 2010 sampling. I chose these sites because they are located near continuous monitoring of water chemistry via sondes (including temperature, turbidity, conductivity, dissolved oxygen, and pH) by other research programs at UNM (Van Horn et al., 2006; Hall et al., 2009). High streamflow present in late April, commonly caused by tributary influx from snow melt, forced me to choose the two alternate transects, Bernalillo T4 and Alameda T5 (Figures 27 and 28).

Due to the presence of Cochiti Dam upstream of my sampling reach, substrate size can change dramatically as one moves downstream from US Route 550 (cobbles, $>5\ cm$) to Alameda Blvd. (sand, $\sim 1000 - 2000\ \mu m$) (Ortiz, 2004). The sediment coarsening found in the upper part of the reach is due mostly to decreased channel width and increased incision caused in large part by bed load trapping at Cochiti Dam as well as various bank stabilization projects in the Albuquerque area. Downstream, various tributary inflows including arroyos (i.e., Montoyas and Cabezon) and the Albuquerque Metropolitan Arroyo Flood Control Authority (AMAFCA) North Diversion Channel provide sources of finer sediments before the Alameda Blvd. Bridge (Swanson et al., 2011). However, the Bernalillo side-channel transect, Bernalillo T3,

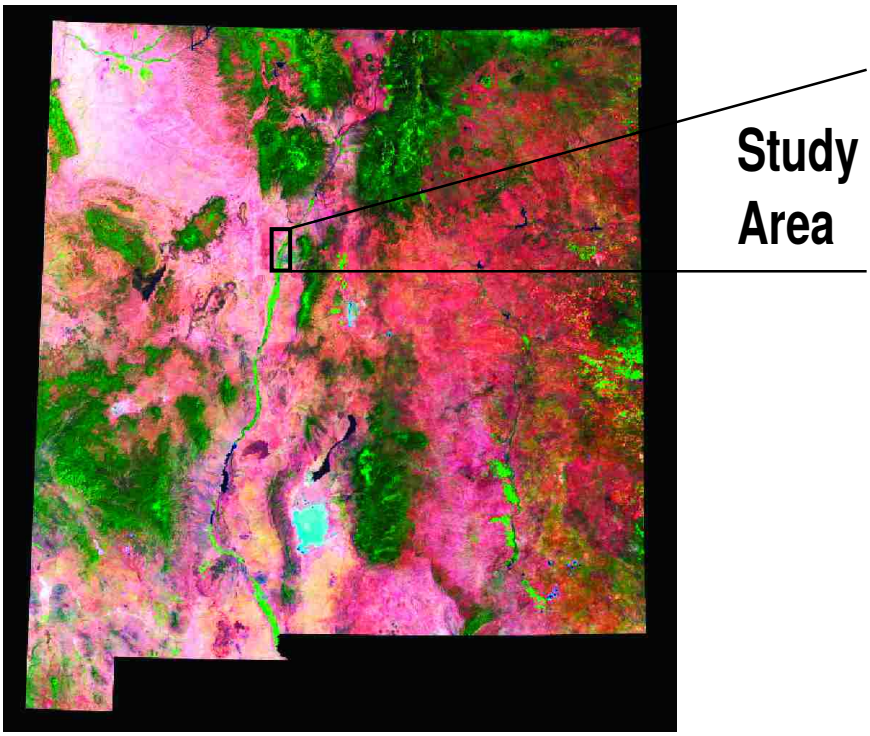

Figure 1: Map of middle Rio Grande study area. Black rectangle delineates study area on this Landsat image of New Mexico, USA.

is located on the opposite side of an island, which is in roughly the same whole-river transect as Bernalillo T2, where there is a shallow side channel with much lower average flow velocity, facilitating the deposition of finer sediments and a silty substrate (the island forms the right edge of water in the main channel transect and the left edge of water in the side-channel transect). The Bernalillo transects, particularly the main-channel transect Bernalillo T2, generally exhibit the lowest turbidity and the main-channel transect generally has the highest flow velocities in this study. By the time water reaches the Alameda Blvd. Bridge, decreased flow velocities and the influx of finer sediments from sources mentioned above (i.e., the AMAFCA North Diversion Channel and various arroyos) facilitate the presence of the sandy substrate characteristic of the Alameda location (Alameda T1 and Alameda T5).

As mentioned, the primary transects where I took most measurements are Alameda T1 (generally a sand substrate), Bernalillo T2 (generally a cobble substrate) and Bernalillo T3 (generally a silt substrate). However, very high flows during one of the

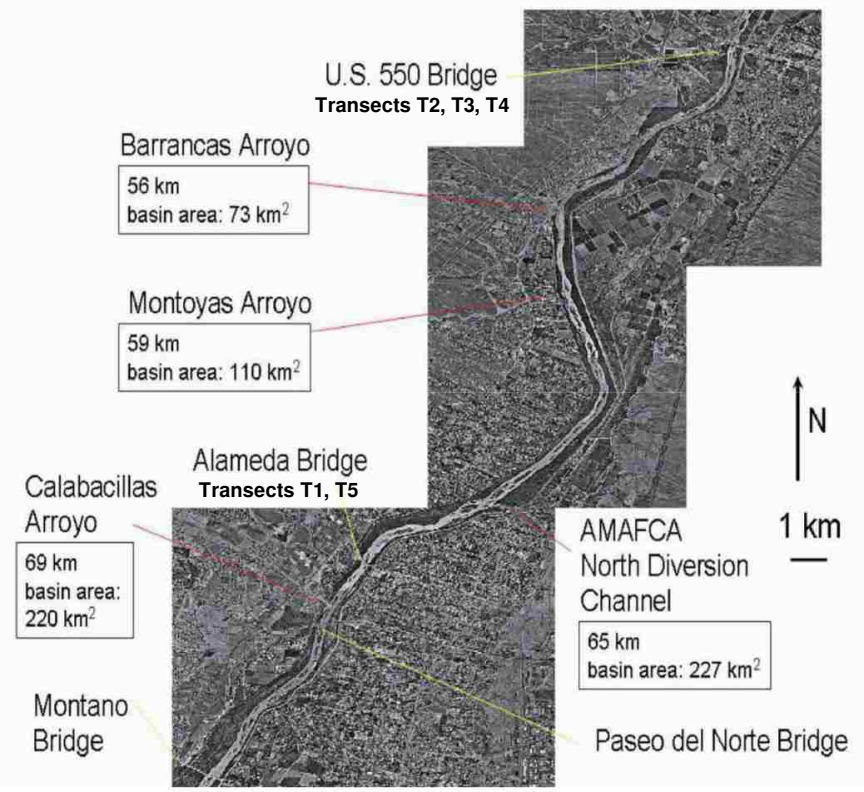

Figure 2: Mosaic of USGS air photos of the study reach. The reach extends from U.S. 550 Bridge in Bernalillo in the north to Montaño Bridge in the south. Length of reach is 25.5 river kilometers. Resolution is 16 meters. (Ortiz (2004), Figure 1). The upstream transects Bernalillo T2, T3, and T4 are near the US Route 550 Bridge (upper photo) and the downstream transects Alameda T1 and T5 are located near the Alameda Blvd. Bridge (lower photo).

sample periods (24 & 25 April 2010) in the main-channel transects (Alameda T1 and Bernalillo T2) required the substitution of alternate nearby transects (main-channel transect Bernalillo T4 and island-side-channel transect Alameda T5).

A U.S. Geological Survey (USGS) gauging station is located at the Alameda Blvd. Bridge and provides continuous measurement of discharge (Turnipseed and Sauer, 2010) and, for this study, I calculated discharge at each transect using my own measurements and standard USGS methods (see below (Rantz, 1982).

I recorded the locations of transects, including elevation and coordinates of the left and right edges of water, using a Garmin GPSMAP 76 Global Positioning System (GPS) device. Finally, I took photographs to document the state of each transect during sampling, along with any noteworthy phenomena.

The Universal Transverse Mercator (UTM) coordinates using the North American Datum of 1983 (NAD83) for the left edges and right edges of water (LEWs and REWs) for each transect on a single sampling date from upstream to downstream are as follows:

Bernalillo T2, 29 March 2010	LEW: 13S 0358390 3909793	REW: 13S 0358367 3909824
Bernalillo T3, 31 March 2010	LEW: 13S 0358330 3909859	REW: 13S 0358325 3909860
Bernalillo T4, 24 April 2010	LEW: 13S 0358441 3909772	REW: 13S 0358385 3909778
Alameda T1, 28 March 2010	LEW: 13S 0350568 3896089	REW: 13S 0350492 3896142
Alameda T5, 25 April 2010	LEW: 13S 0350522 3896000	REW: 13S 0350483 3896020

2.2 Water chemistry

I measured water chemistry including temperature, conductivity, total dissolved solids, salinity, dissolved oxygen, barometric pressure, and pH at each transect using a YSI 556MPS handheld multiparameter instrument. I measured turbidity using a LaMotte 2020e turbidity meter. Most of these parameters are known to be important for many species of benthic algae including diatoms, and many species have relatively narrow ranges in which they are found (Van Dam et al., 1994; Potapova and Charles, 2002). Although physicochemical parameters can vary significantly at larger scales in lotic

systems (Poff and Ward, 1990), I assume that the water chemistry does not vary significantly across a given transect. I made this assumption based on preliminary measurements of turbidity that I took across the proposed main channel transect near US Route 550 in Bernalillo, which showed no significant variability. As such, I measured water chemistry only once during a given sampling date at each location.

2.3 Flow velocity and discharge

I used standard USGS methods to measure flow velocity and discharge (Rantz, 1982). I divided transects into cells, each containing roughly 5% of the total discharge (20 to 25 cells per transect). Before sampling I identified areas suspected to contain large proportions (i.e., thalweg) or small proportions (i.e., edges) of the total discharge because I did not know discharge rates beforehand. I did this by creating a bed profile before sampling. I delineate verticals at the center of each cell, as well as the relative locations of the left (LEW) and right edges of water (REW) using a fiberglass tape measure spanning the transect. I measured depth and velocity at verticals in the center of each cell using a top-setting wading rod. At verticals that are less than 76 *cm* deep, I measured velocity at 20%, 60% and 80% of the total depth and at verticals deeper than 76 *cm*, I measured velocity at 20% and 80% of the depth. I measured flow velocity within each cell using a Marsh-McBirney, Inc. Flo-Mate Model 2000 portable flowmeter equipped with an electromagnetic sensor. I calculated discharge by multiplying the velocities taken at each vertical by the area of their respective cells, then adding all of the cell discharges to produce total discharge in the transect.

2.4 Chlorophyll *a*

I took shallow sediment cores (sand and mud) or rock scrubs (cobbles) at each of the discharge-measurement cells located along the transect (20 to 25 locations per transect). I took additional samples near the edges when necessary for capturing

variation across transects; if edge gradients are low, sampling only within cells by percent of discharge may produce insufficient sampling at edges. Due to high flow and depth during occasional sampling events I was unable to take benthic samples at every cell location for which I measured velocity. However, this was infrequent and I do not expect it to significantly change my results.

I sampled sediment cores using a 2.5 cm diameter by 5 mm deep syringe. At each sample location I took 3 cores, and stored them in a 50 ml centrifuge tube, wrapped them in foil and placed the samples on ice until extraction. I used a Loeb sampler (adapted from Loeb (1981) to take 2.6 cm diameter circular rock scrubs of cobbles. I took 2 scrubs per sample location and stored samples in half-pint canning jars wrapped in foil, placed on ice and then they were filtered using 0.7 μm glass fiber filters in the lab prior to the extraction of pigments for chl a characterization.

I used a hot ethanol method adapted from Sartory and Grobbelaar (1984) to extract and measure chl a (Biggs et al., 1999; Carignan et al., 2000). Chl a was extracted from samples (either sediment from cores or filters from rock scrubs) in 50 ml centrifuge tubes using a known volume of 95% ethanol (usually 10 ml) by shaking, then heating in a 79 °C water bath for five minutes followed by 24 hours in the dark. Then roughly 1 ml of the extractant was pipetted into a cuvette for spectrophotometric analysis of light absorption at 665 and 750 nm using a Cary 50 Scan UV/Vis scanning spectrophotometer. Following the initial measurement of absorption, I added 0.1 ml of 0.1 N HCl to each cuvette. After allowing 90 seconds for complete pheophytinization of the chl a, the absorption measurements were taken again. I calculated the amount of chl a in mg/m^2 using the following formula:

$$\text{Chl } a = \frac{K(665_o - 665_a)v}{\ell A} \tag{1}$$

where 665_o is the absorption at 665 nm before the addition of acid with absorption

at 750 nm subtracted out and 665_a is the absorption at 665 nm after the addition of the acid with absorption at 750 nm subtracted out, v is the volume of extractant used (in liters), A is the area of benthos sampled in m^2, and ℓ is the path length of the cuvette in cm (1 cm). K (28.78) is a coefficient that accounts for the absorption coefficient of chl a and has units of $(cm \cdot mg)/L$ (Lorenzen, 1967).

2.5 Irradiance

To estimate light availability at the surface of the water, I used data collected by the National Oceanographic and Atmospheric Administration's (NOAA) Integrated Surface Irradiance Study (ISIS) (Hicks et al., 1996). The data collection site is located at the National Weather Service site near the Albuquerque International Airport and instrumentation mounted on the Albuquerque solar tracker include a total solar pyranometer, a diffuse pyranometer, and a UV-B biometer. Data have been collected covering the entire range of my sampling period (January through August, 2010) and the data are reported as 3-minute averages of one-second samples. I further averaged the data to obtain daily mean irradiance and also calculated daily maximum irradiance.

2.6 Data analysis

All data analyses and plots were produced using the R statistical computing language and environment version 3.2.2 (R Core Team, 2015). In addition to the base R packages, the 'lattice' package (version 0.20-33) was used to produce trellis plots in Figure 6 (Sarkar, 2008), the 'xtable' package (version 1.7-4) was used to generate the LaTeX code for Table 1 (Dahl, 2014), and the 'knitr' package (version 1.11) was used to integrate the results of the R code into the LaTeX code for typesetting (Xie, 2015b,a, 2014).

2.6.1 Stepwise AIC model selection

In an effort to better understand the relative importance of the factors that influence chl *a* concentration in this system, I produced a multivariate linear regression method that I tested for respective out-of-sample prediction error. I developed the model using the following basic linear multivariate form:

$$Y = (\beta_0 X_0) + (\beta_1 X_1) + \ldots + (\beta_n X_n) \tag{2}$$

I selected coefficients for the model by stepwise regression using the Akaike Information Criterion (AIC) (Cavanaugh, 2007). At each "step" of the stepwise analysis a model with the current set of variables is compared to a model with a variable added (forward) or a variable removed (backward). I used a backward stepwise regression analysis for this method. Non-linear relationships between independent variables and the dependent variable were explored using logarithmic transformations of the data. Model validation was performed using a method in which a random subset of 75% of the data was used for the initial model selection (training data) and the remaining 25% (test data) were used to test the out-of-sample prediction error (Figure 23). This method avoids potential overfitting and provides validation for the model selected by stepwise AIC comparison. I used mean absolute error (MAE) to compare the model fits.

3 Results

3.1 Distributions of chl *a* in relation to transect parameters

Figure 3 shows the distribution of chl *a* data in 150-bin histograms for the combined data and for the data associated with each of the main substrate types. The figure shows that the data are right-skewed, with many samples containing relatively low amounts of chl *a*, and fewer measurements with relatively large amounts of chl *a*. To explore the variation in chl *a* with respect to the various parameters measured, I present box-and-whisker plots of chl *a* versus each individual parameter in Figures 4 and 5. In these plots the thicker black line represents the sample median and the box outlines the range of the data between the upper and lower quartiles while the whiskers represent the nominal range of the data inferred by the quartiles, and lastly, the circles represent outliers.

Figure 4 shows the distribution of the amount of chl *a* by three transect characteristics: substrate type, turbidity, and transect. Of particular note, is the much higher mean concentration of chl *a* (delineated by the thicker black bar within the box) seen in the Bernalillo T2 transect, which is the main-channel transect below the US Route 550 Bridge, with a generally cobbled substrate. The substrate plot also shows that the mean chl *a* concentration of the samples taken from the finer sediment silt substrate is higher than that of the sand transects. The turbidity plot, which shows the relationship between turbidity and chl *a* for all of the data, suggests that higher turbidity is associated with lower concentrations of chl *a* at least for all of the data together (see text below and Figures 11, 15, and 19 for breakdowns of turbidity by transect, substrate type, and sampling date).

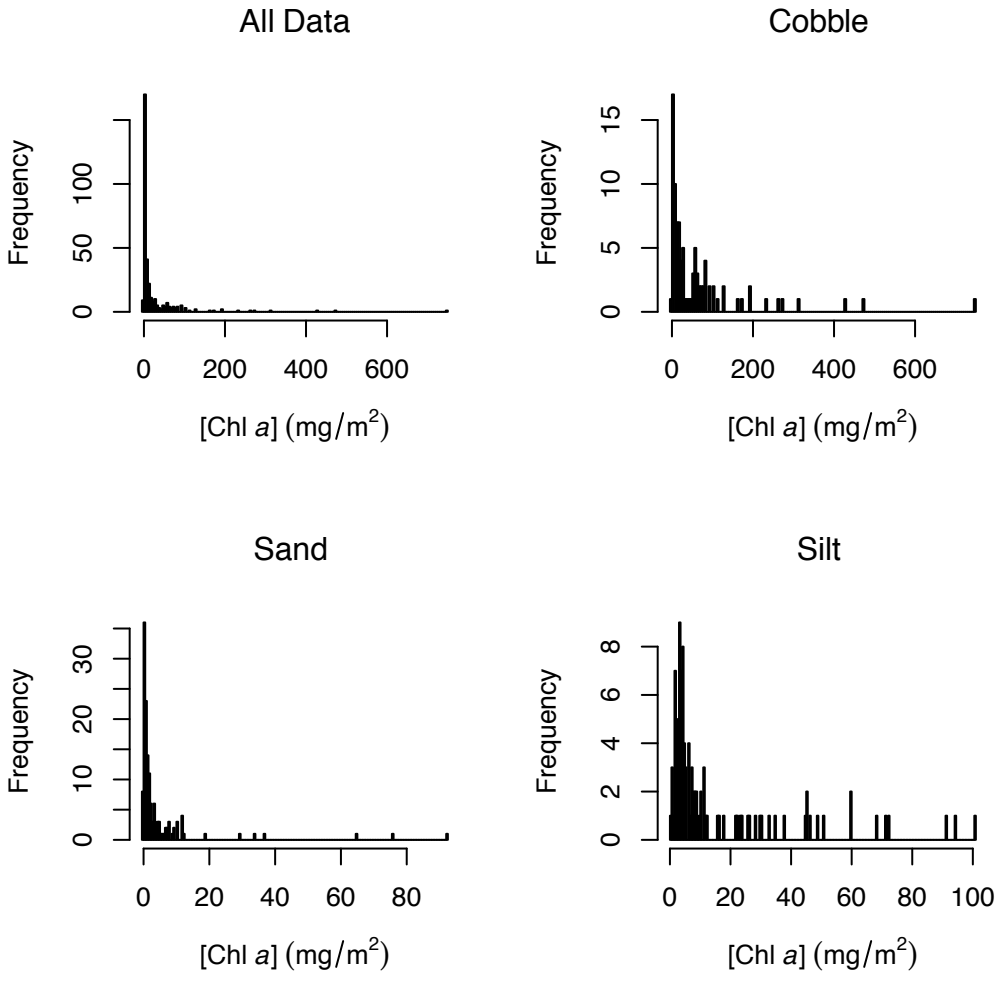

Figure 3: Histograms showing distribution of all chl *a* data and for each substrate type

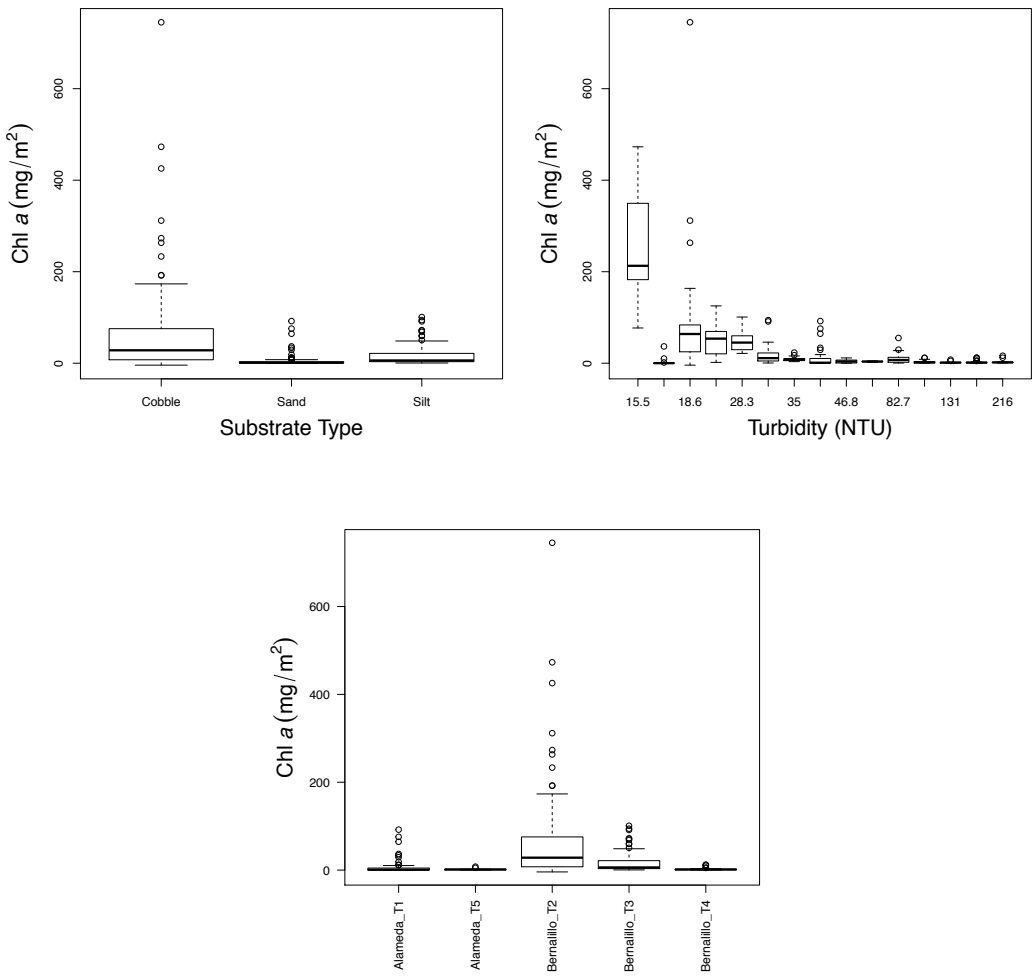

Figure 4: Box plots showing the relationships among various channel parameters and the concentration of chl *a* for all samples. The thicker black line represents the sample median and the box outlines the range of the data between the upper and lower quartiles, while the whiskers represent the nominal range of the data inferred by the quartiles. The circles represent outliers.

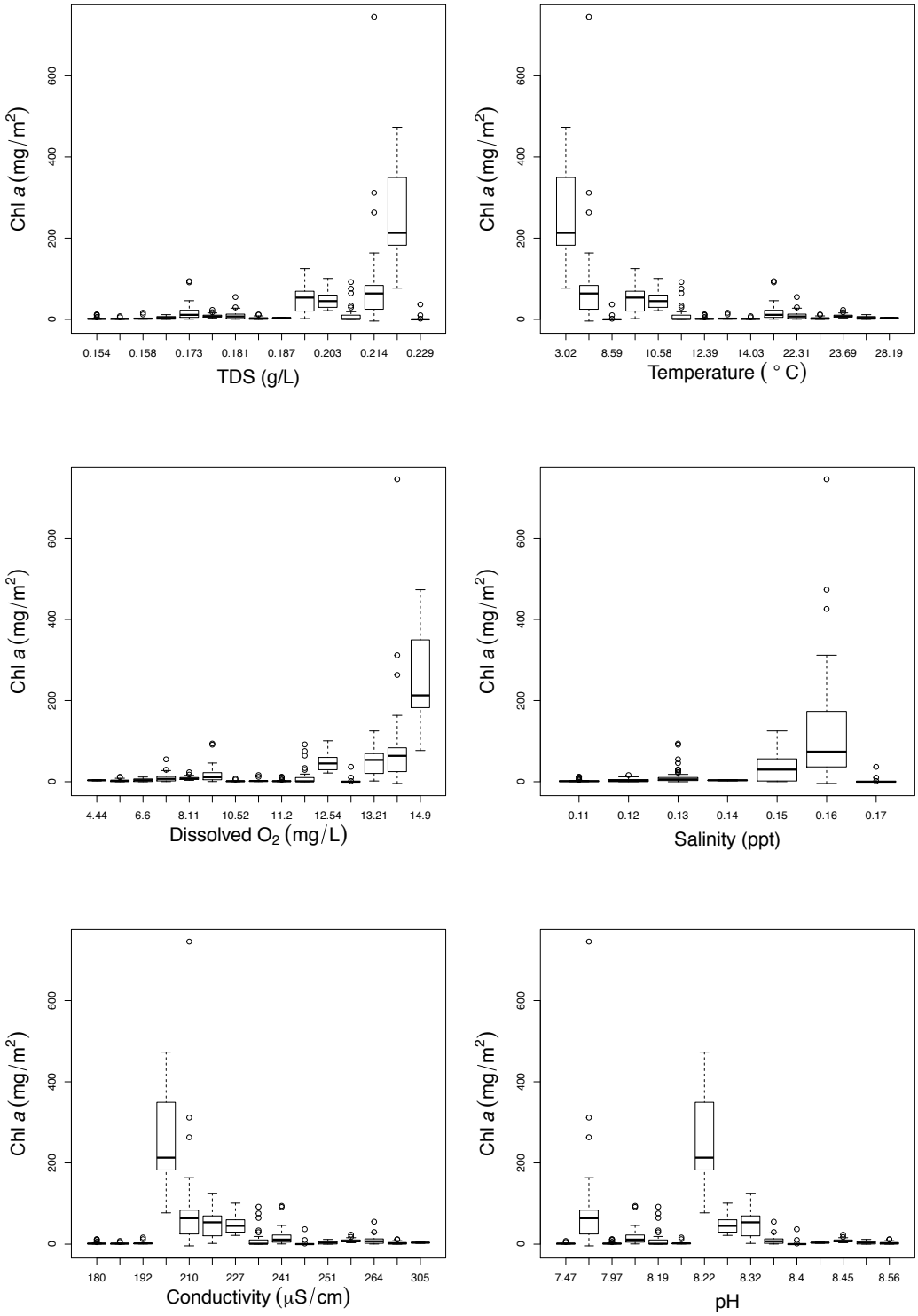

Figure 5: Box plots showing the relationships among the measured water chemistry parameters and the concentration of chl *a* for all samples, see Figure 4 for plot overview.

3.1.1 Chl *a* versus key parameters for each substrate

Figure 6 provides side-by-side comparisons across all of the data for some of the relationships I am most interested in understanding. Some of the patterns of note include those mentioned in the earlier scatter plots but here they are directly compared to one another, and some of the relationships between each of the three main substrate types and chl *a* are easier to see. The stacked pattern that we see in the turbidity plot is due to the single measurement of turbidity (as was done with the other water chemistry parameters) corresponding to the range of different chl *a* measurements taken during each sampling date at respective transects. Figures 11, 15, and 19 show the turbidity data by substrate, transect, and sampling data.

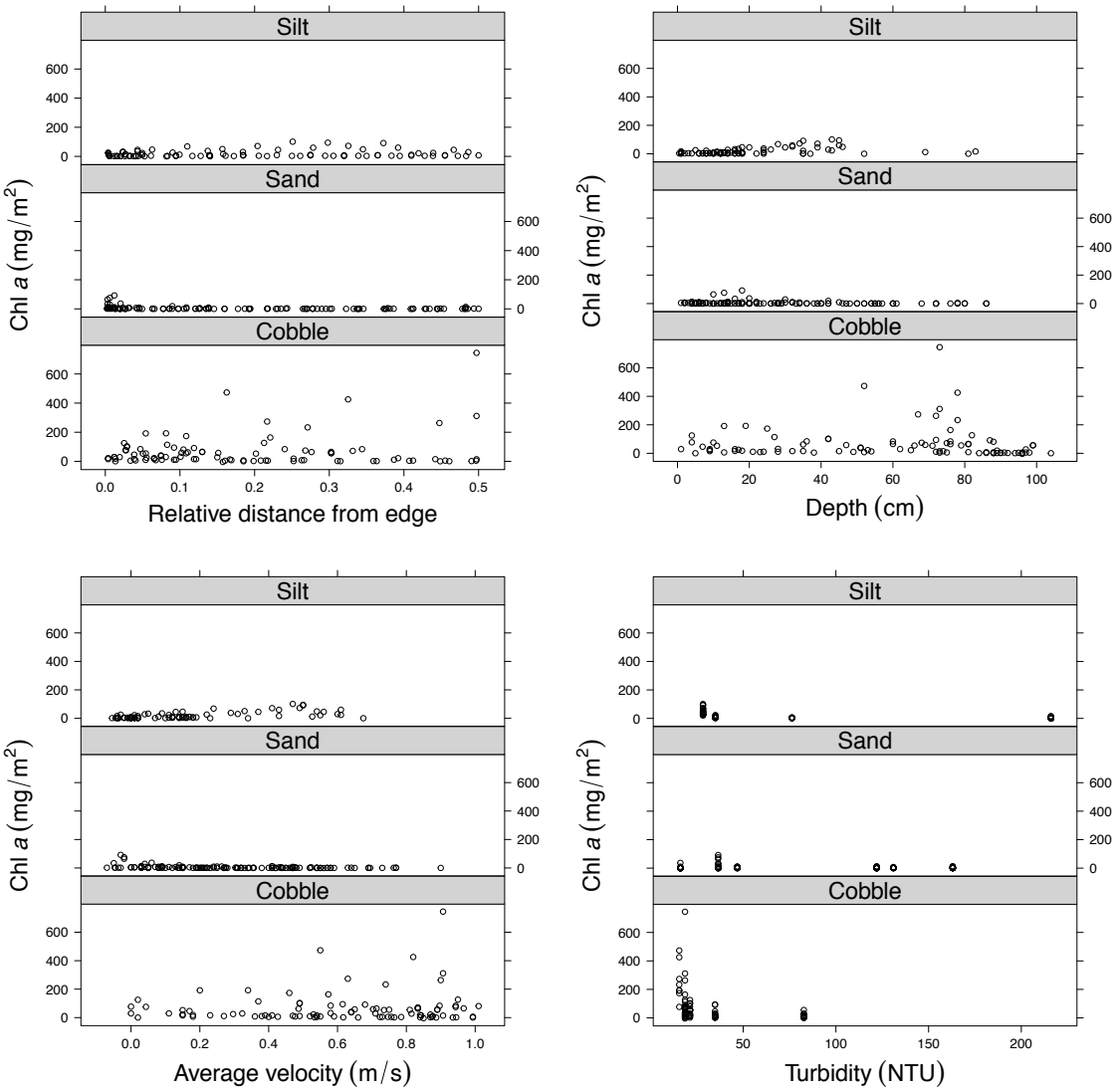

Figure 6: Scatter plots of chl *a* vs. relative distance from an edge, depth, average velocity, and turbidity by substrate type for all transects

3.1.2 Trends by substrate type, sampling date, and transect

Figure 7 provides a look at chl *a* values versus distance from an edge for each of the main substrate types as scatter plots with linear fits. The fitted lines have low R^2 values for all of these plots, indicating a poor linear correlation between distance from an edge and the amount of chl *a*. However, it is still worth noting that the sand transect plot clearly shows the hypothesized pattern of edge-related production (Figure 7). Although the relationship is not linear, the highest concentrations of chl *a*

are only found at relatively short distances from an edge, possibly because of higher sediment turnover as the result of generally higher flow velocities toward the middle of the transect. The other two plots show significant amounts of chl *a* at relatively large distances from an edge indicating that other factors (i.e., depth, flow velocity, bed mobility, differences in algal taxa, or differences in grazing by algivores) likely influence the amount of algae in those environments (Figure 7).

Relationships among key explanatory variables (relative distance, depth, velocity, and turbidity) and chl a concentrations vary among sampling dates for each transect. I explored these relationships by plotting $\log_e$ transforms of the response variable (chl *a*) with linear fitted lines for each of the explanatory variables that were measured at various points across the transect (distance, depth, and velocity). These relationships for the main-channel sand transect, Alameda T1, and the alternate main-channel transects, Bernalillo T4 and Alameda T5, are shown in Figures 8, 9, and 10. The data are presented in the same manner for the main-channel cobble transect, Bernalillo T2, and the side-channel silt transect, Bernalillo T3 (Figures 12, 13, 14, 16, 17, and 18). Turbidity was only measured once at each transect during each sampling and those data are presented as plots of the relationship between the measured turbidity and the average concentration of chl *a* with error bars displaying the variance as one standard deviation about the mean (Figures 11, 15, 19).

For the distance data at the sand substrate transects, log-transforms generally provide better linear fits compared to the untransformed aggregate data shown in Figure 7. A negative relationship between relative distance from an edge and the concentration of chl *a* is seen in all but the plot of the Bernalillo alternate transect T4 sampled on 24 April 2015 at the northern end of the reach and this area generally displays different patterns of distance and chl *a* concentration (Figure 7). Similarly negative trends are generally seen in the plots of depth and average flow velocity (Figures 9 and 10). These patterns are expected since depth and flow velocity are

strongly correlated, and increased velocity facilitates bed transport while increased depth decreases available light. The turbidity data for the sand substrate alone does not show a strong pattern, as similar chl *a* values are seen at even the highest values of turbidity measured. This pattern may be caused by the veritable absence of chl *a* in deep sections of these transects except for the alternate transect, Bernalillo T4 (see transect profiles below, Figures 20, 21, and 22).

The cobble and silt transects generally show less negative relationships between distance, depth, and velocity with some fits even suggesting positive relationships, while others are more similar to the sand transects (Figures 12, 13, 14, 16, 17, and 18). Both the cobble and the silt transects show more obvious patterns of decreasing chl *a* concentration with increasing turbidity (Figures 15, 19) These trends may suggest that sampling time can play a larger role in the Bernalillo area, perhaps do to increased sensitivity to changes in depth, velocity, and turbidity.

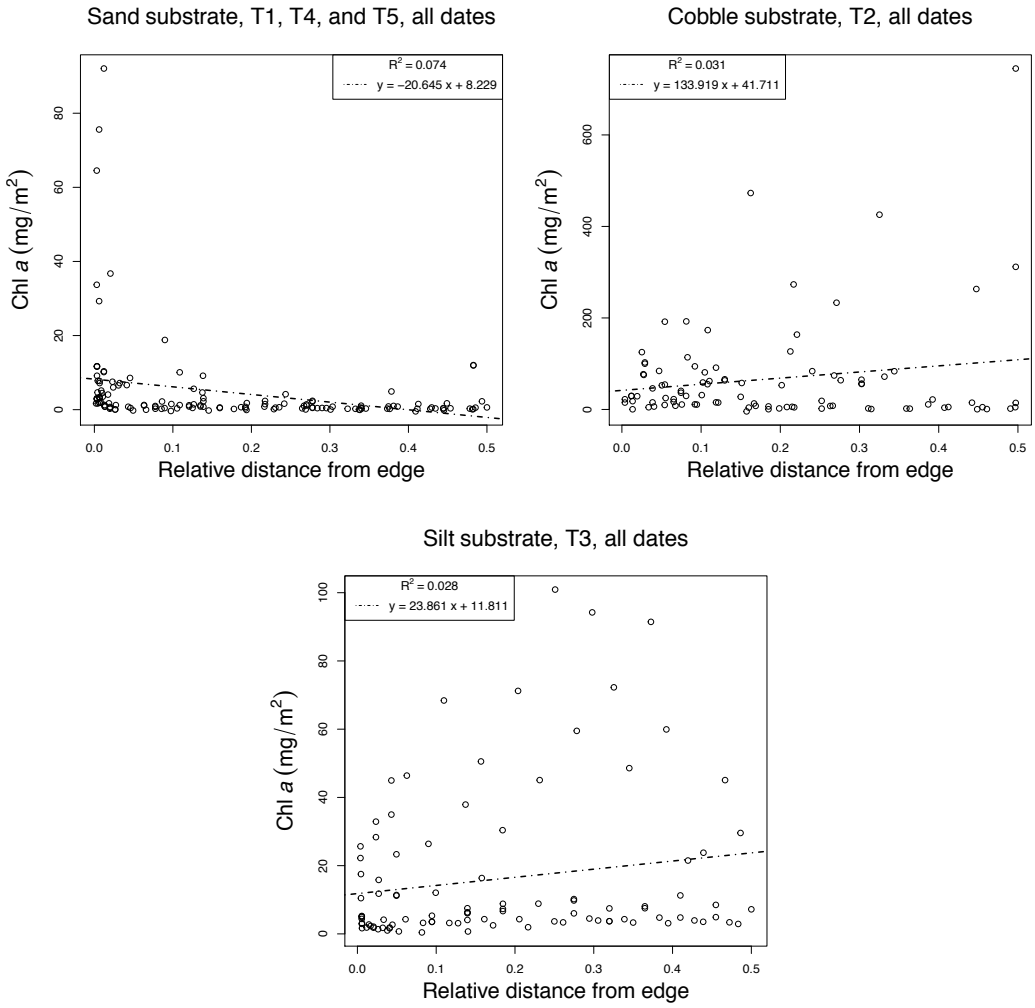

Figure 7: Scatter plots showing the relationship between relative distance from an edge and the concentration of chl *a* in all of the transects for each substrate type with a linear model fitted lines.

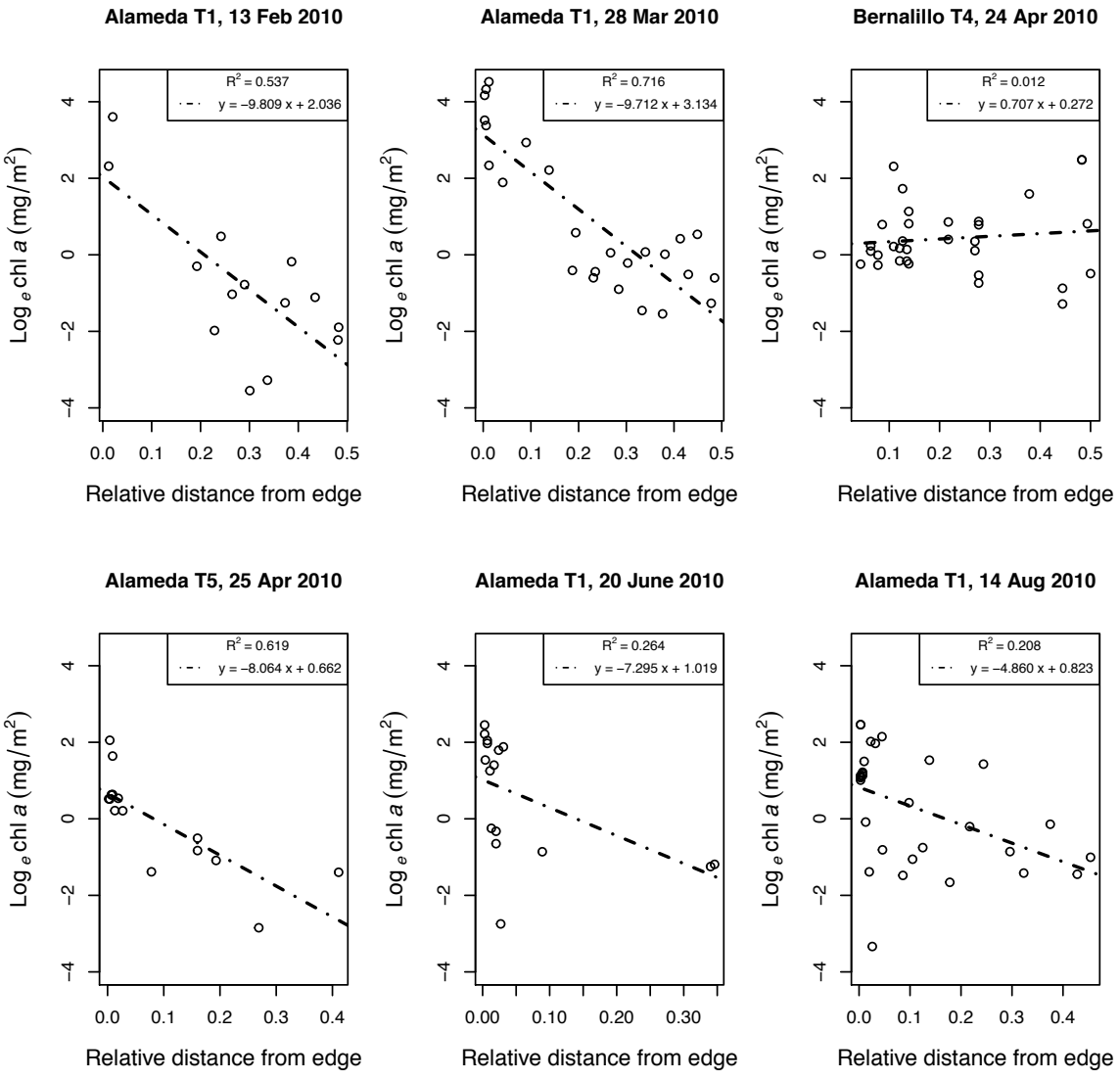

Figure 8: Scatter plot showing the relationships between relative distance from an edge and the concentration of chl *a* in the sand substrate samples with log-transformed y-axis and linear model fitted lines.

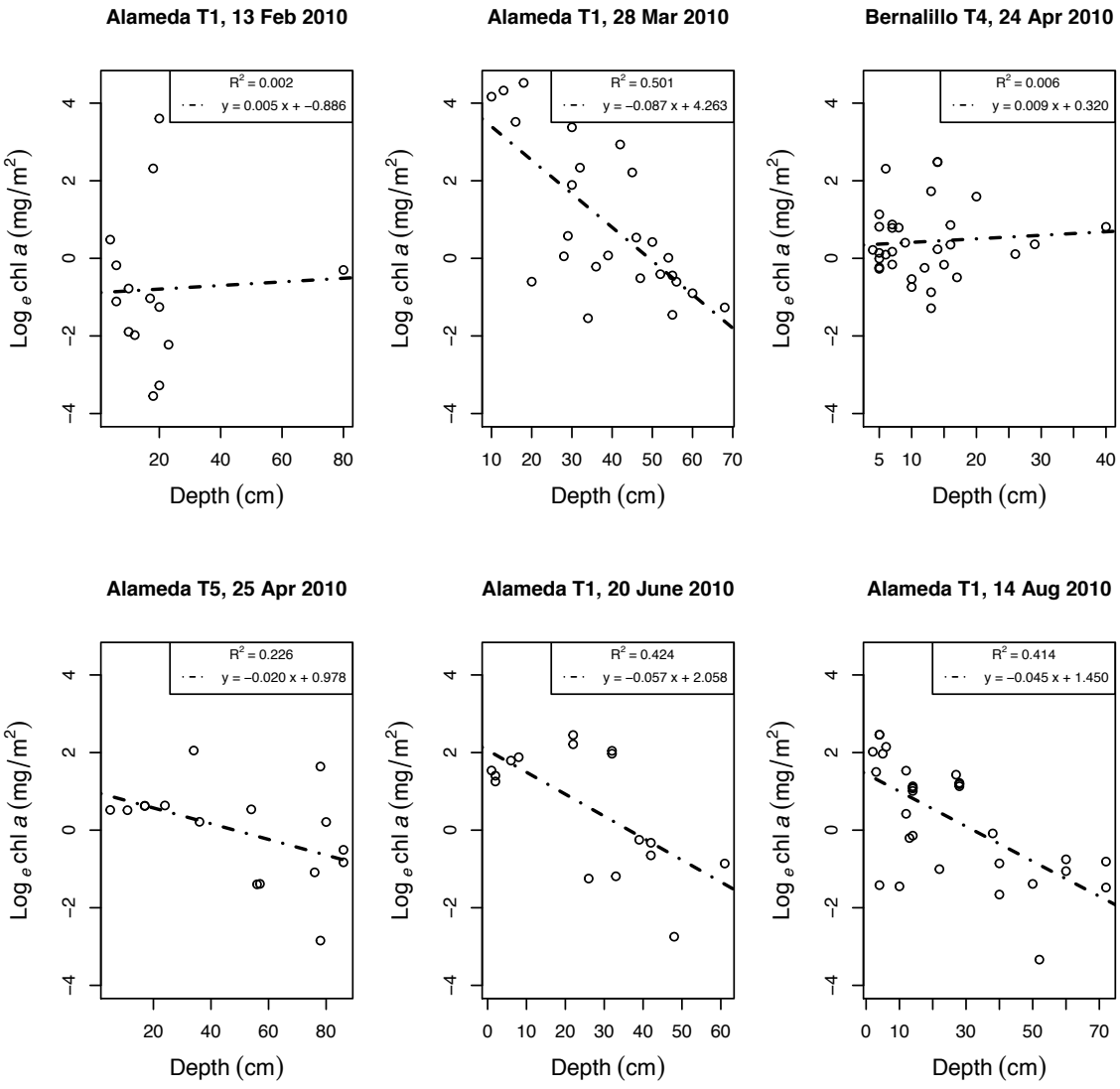

Figure 9: Scatter plots showing the relationships between relative distance from an edge and the concentration of chl *a* in the sand substrate samples with log-transformed y-axis and linear model fitted lines.

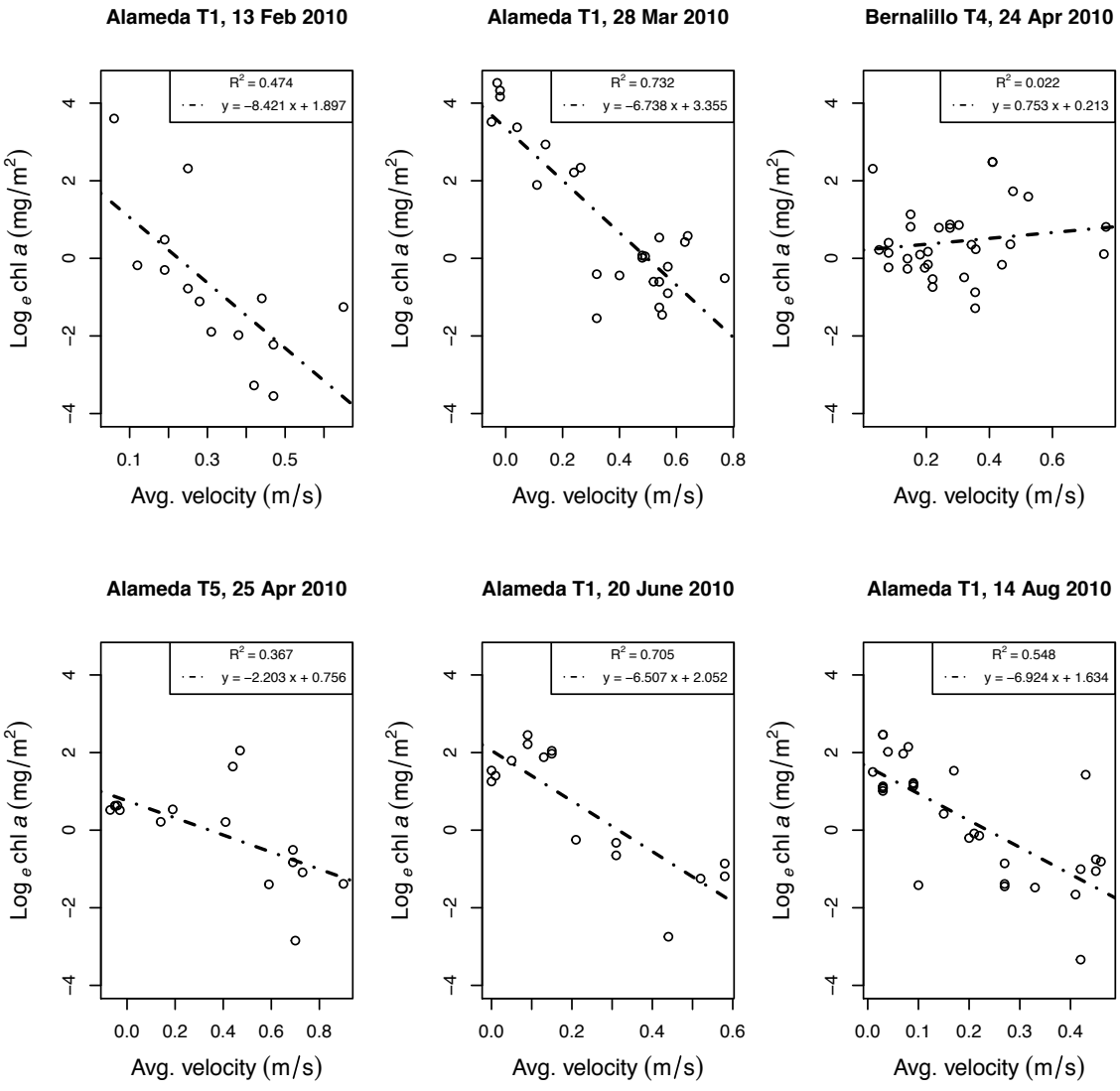

Figure 10: Scatter plots showing the relationships between average velocity (averaged over depth) and the concentration of chl a in the sand substrate samples with log-transformed y-axis and linear model fitted lines.

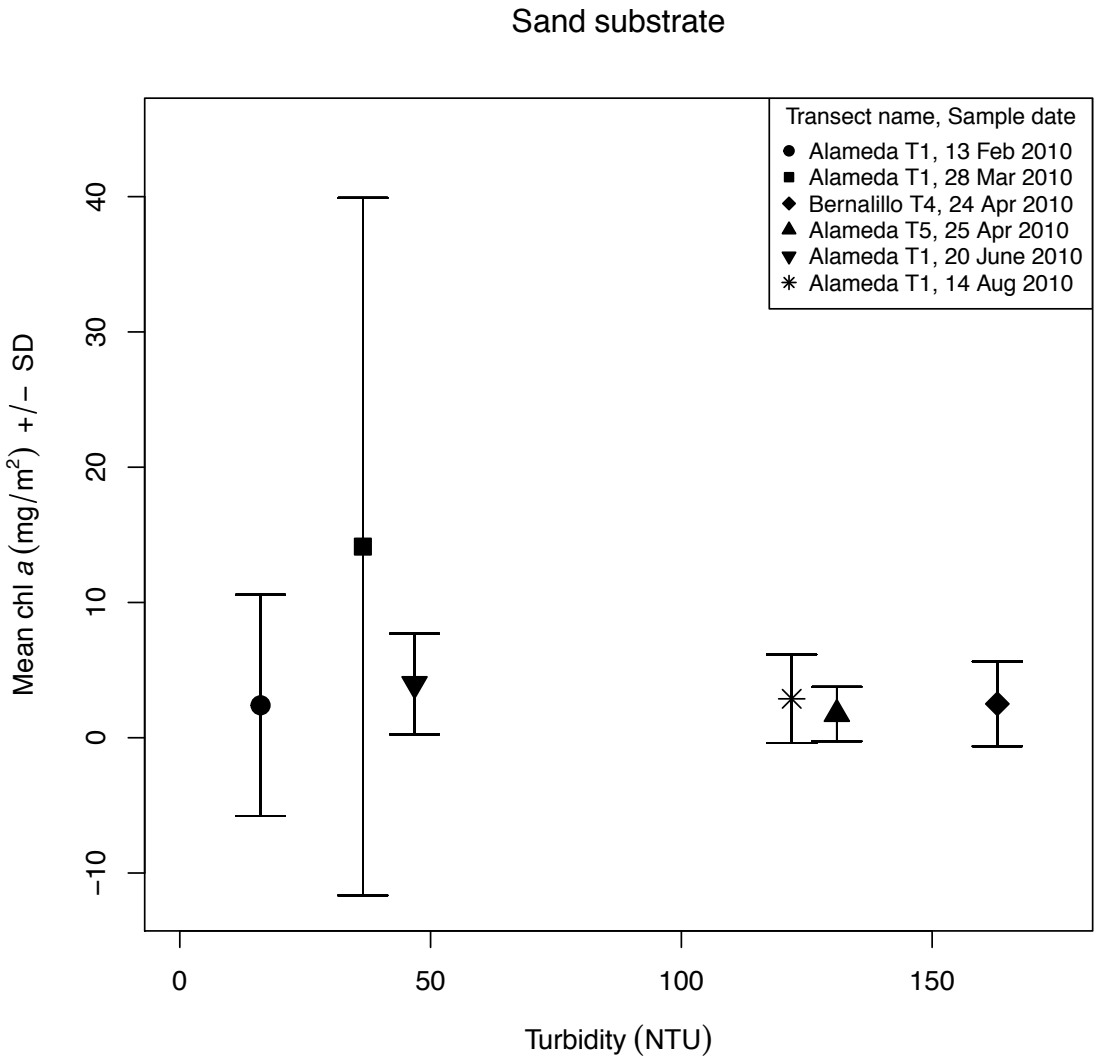

Figure 11: Scatter plot showing the relationship between turbidity and the concentration of chl *a* in the sand substrate samples with error bars showing one standard deviation about the mean.

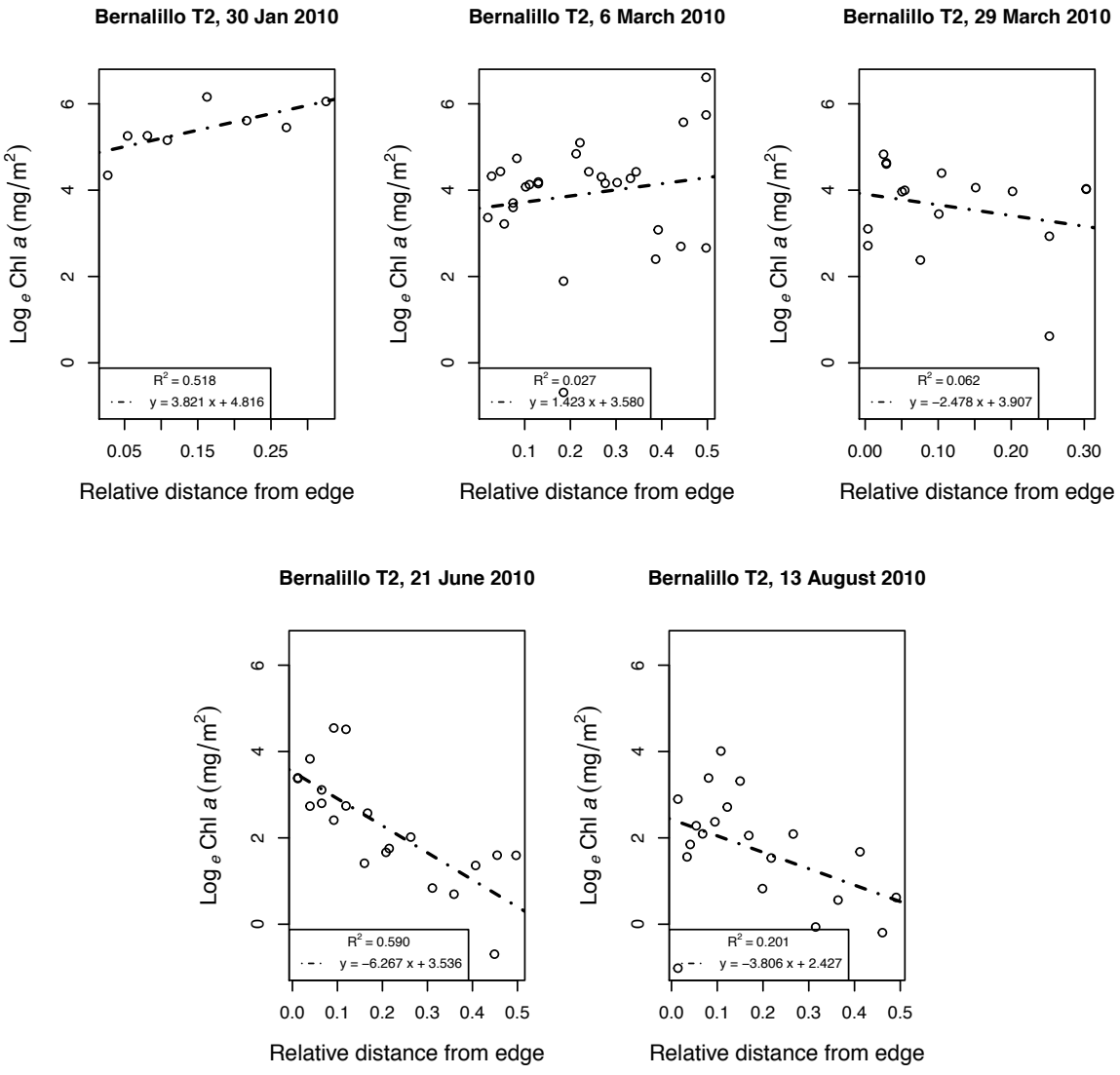

Figure 12: Scatter plots showing the relationships between relative distance from an edge and the concentration of chl *a* in the cobble substrate samples with linear model fitted lines.

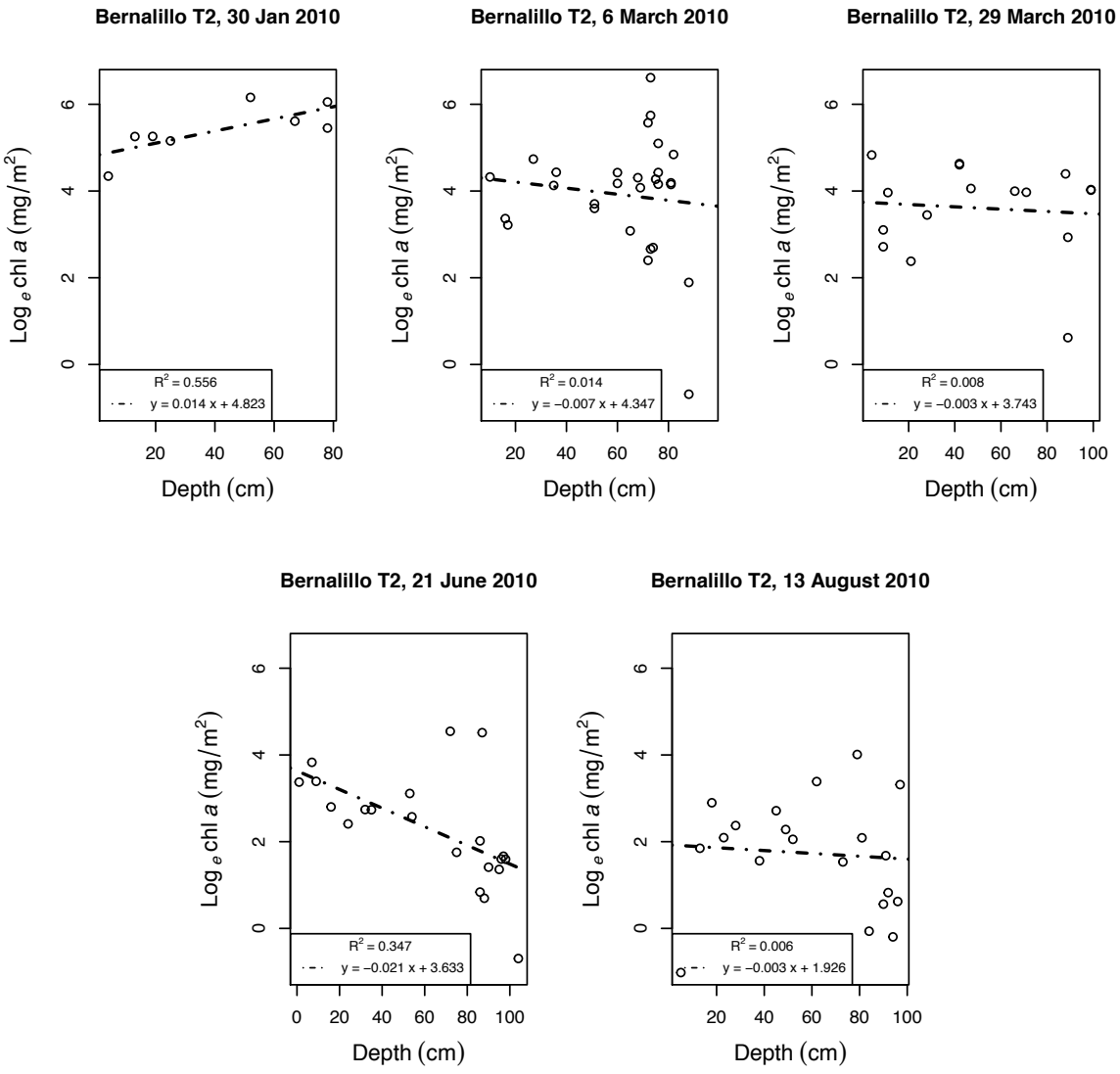

Figure 13: Scatter plots showing the relationships between depth and the concentration of chl *a* in the cobble substrate samples with linear model fitted lines.

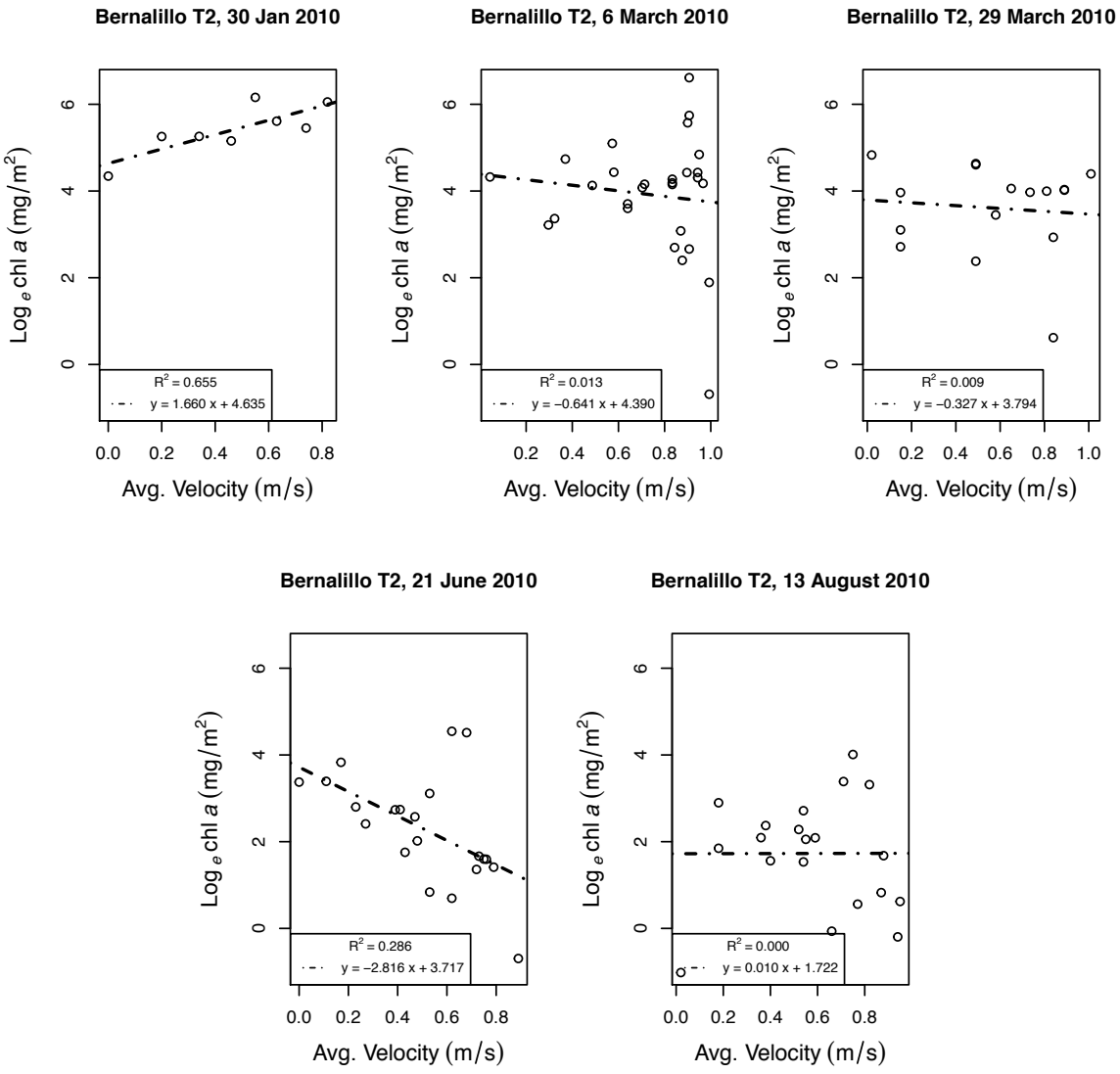

Figure 14: Scatter plots showing the relationships between average velocity (averaged over depth) and the concentration of chl a in the cobble substrate samples with linear model fitted lines.

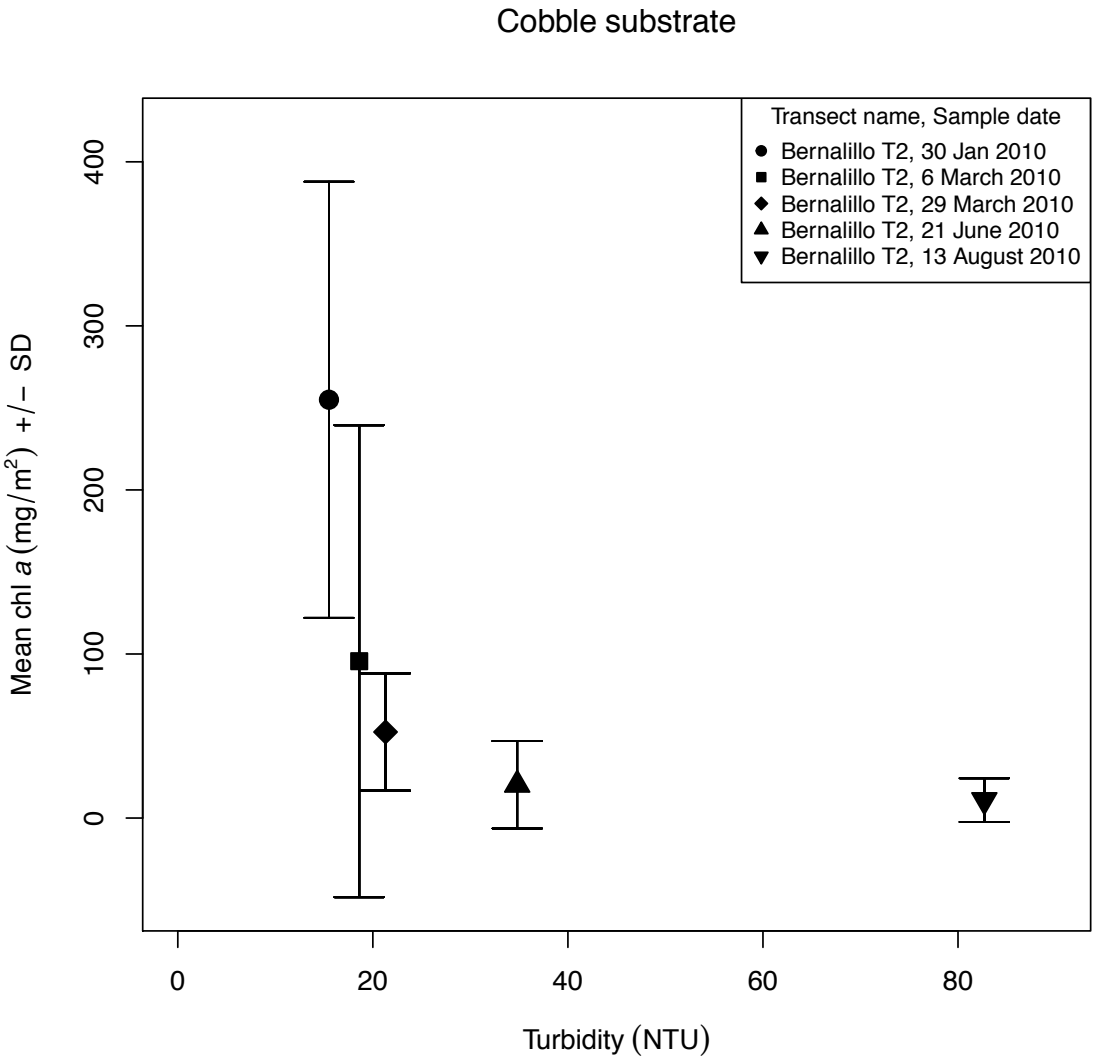

Figure 15: Scatter plot showing the relationship between turbidity and the concentration of chl *a* in the cobble substrate samples with error bars showing one standard deviation about the mean.

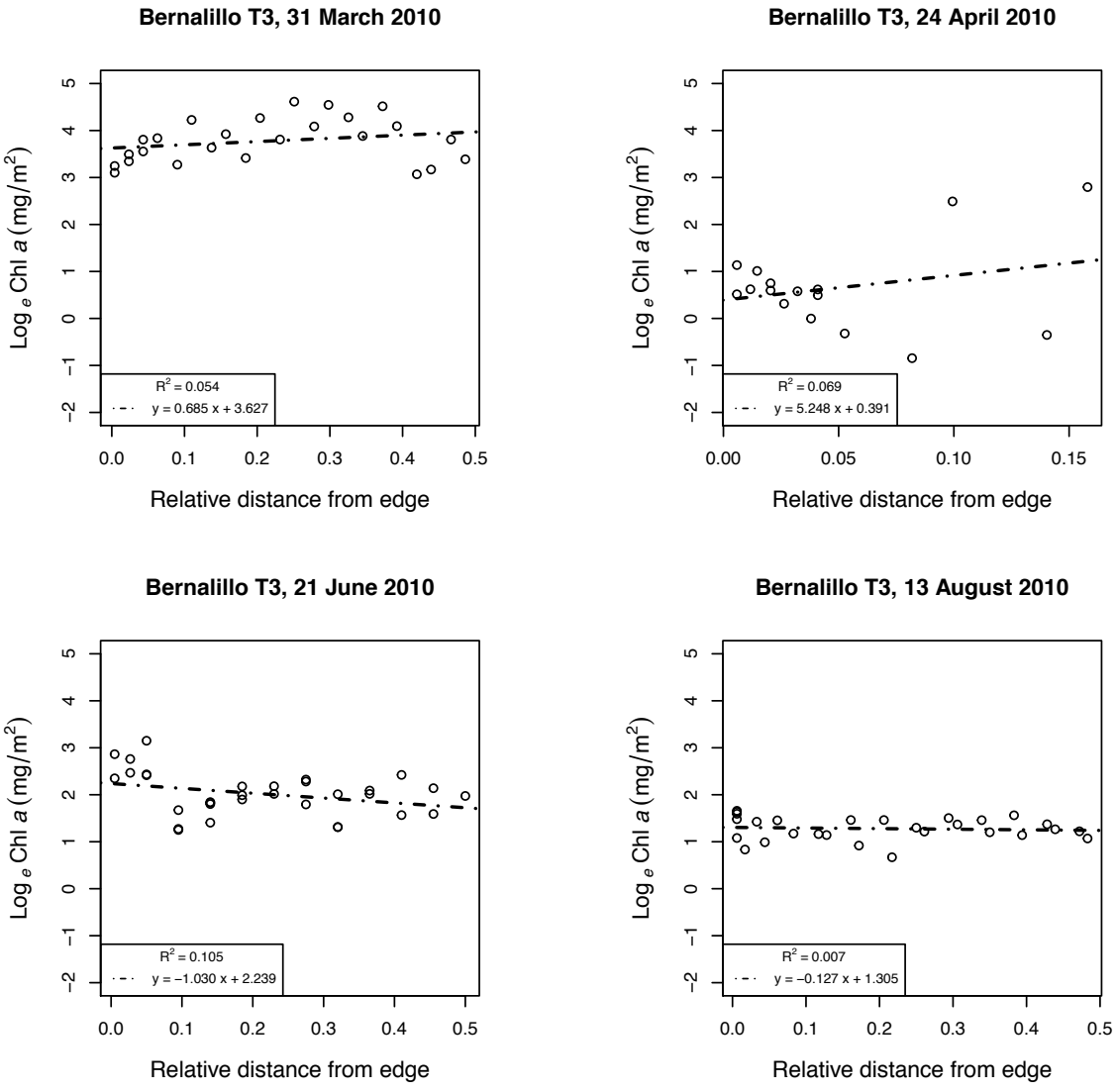

Figure 16: Scatter plots showing the relationships between relative distance from an edge and the concentration of chl *a* in the silt substrate samples with log-transformed y-axis and linear model fitted lines.

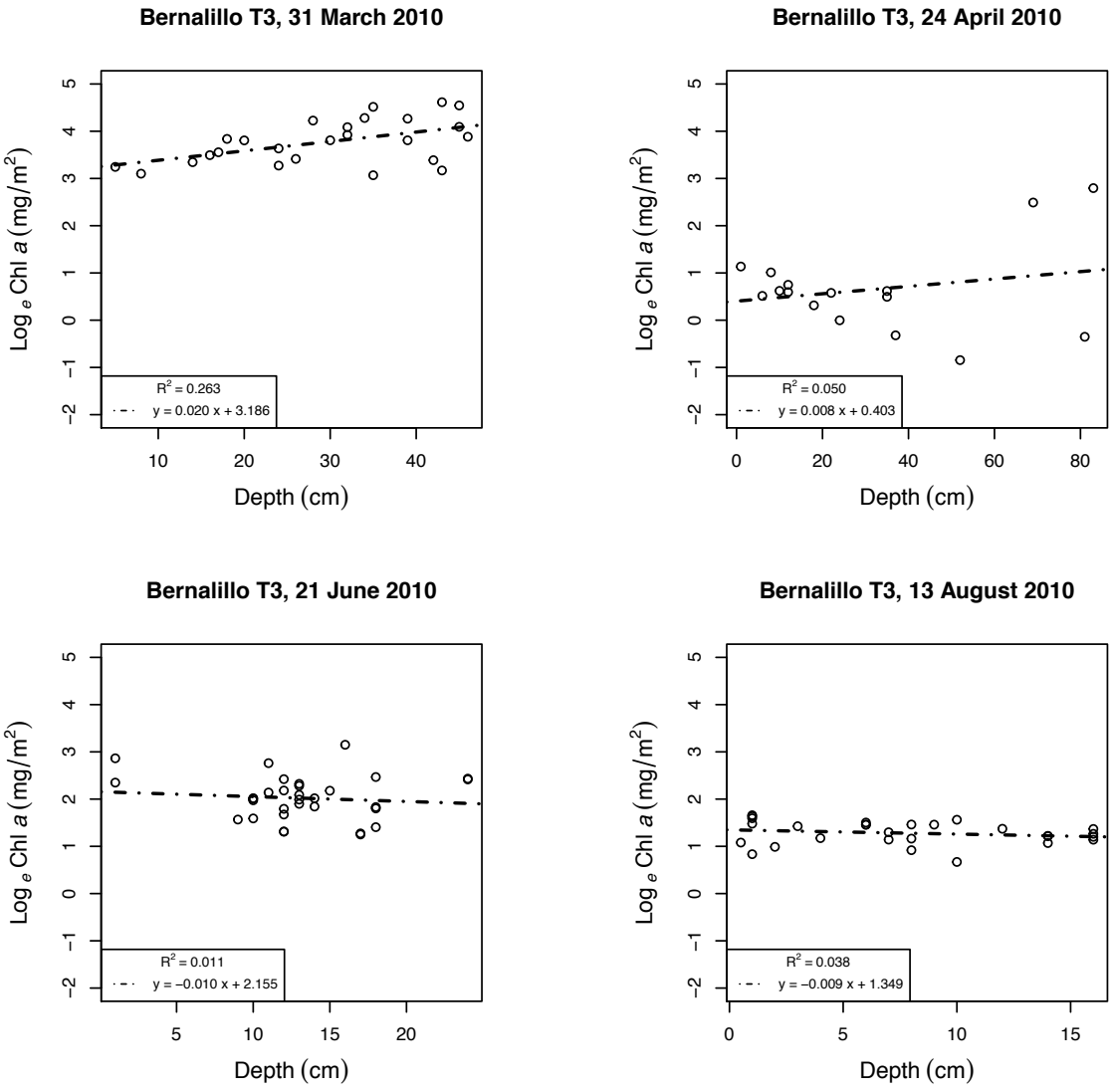

Figure 17: Scatter plots showing the relationships between depth and the concentration of chl *a* in the silt substrate samples with log-transformed y-axis and linear model fitted lines.

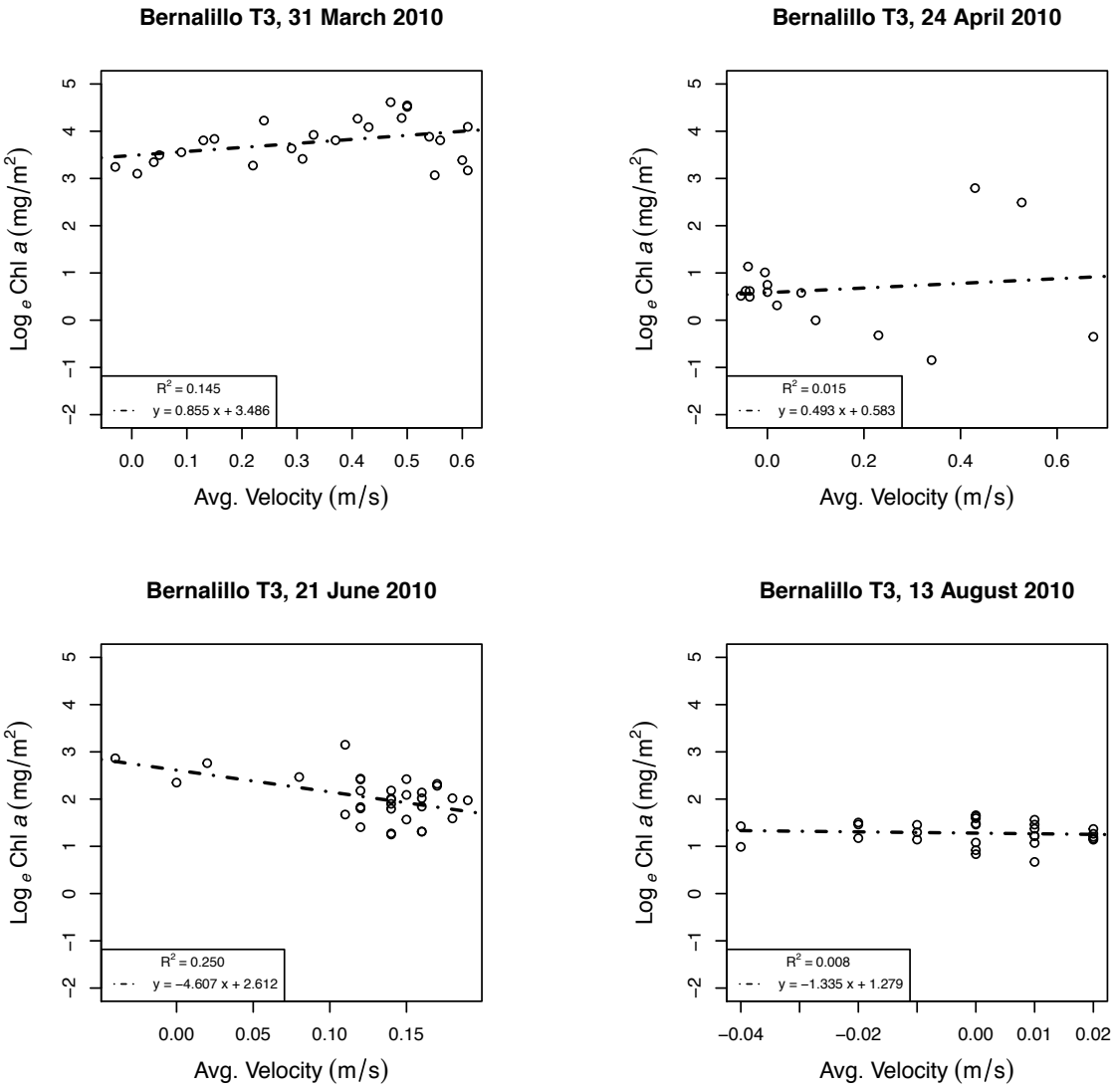

Figure 18: Scatter plots showing the relationships between average velocity (averaged over depth) and the concentration of chl *a* in the silt substrate samples with log-transformed y-axis and linear model fitted lines.

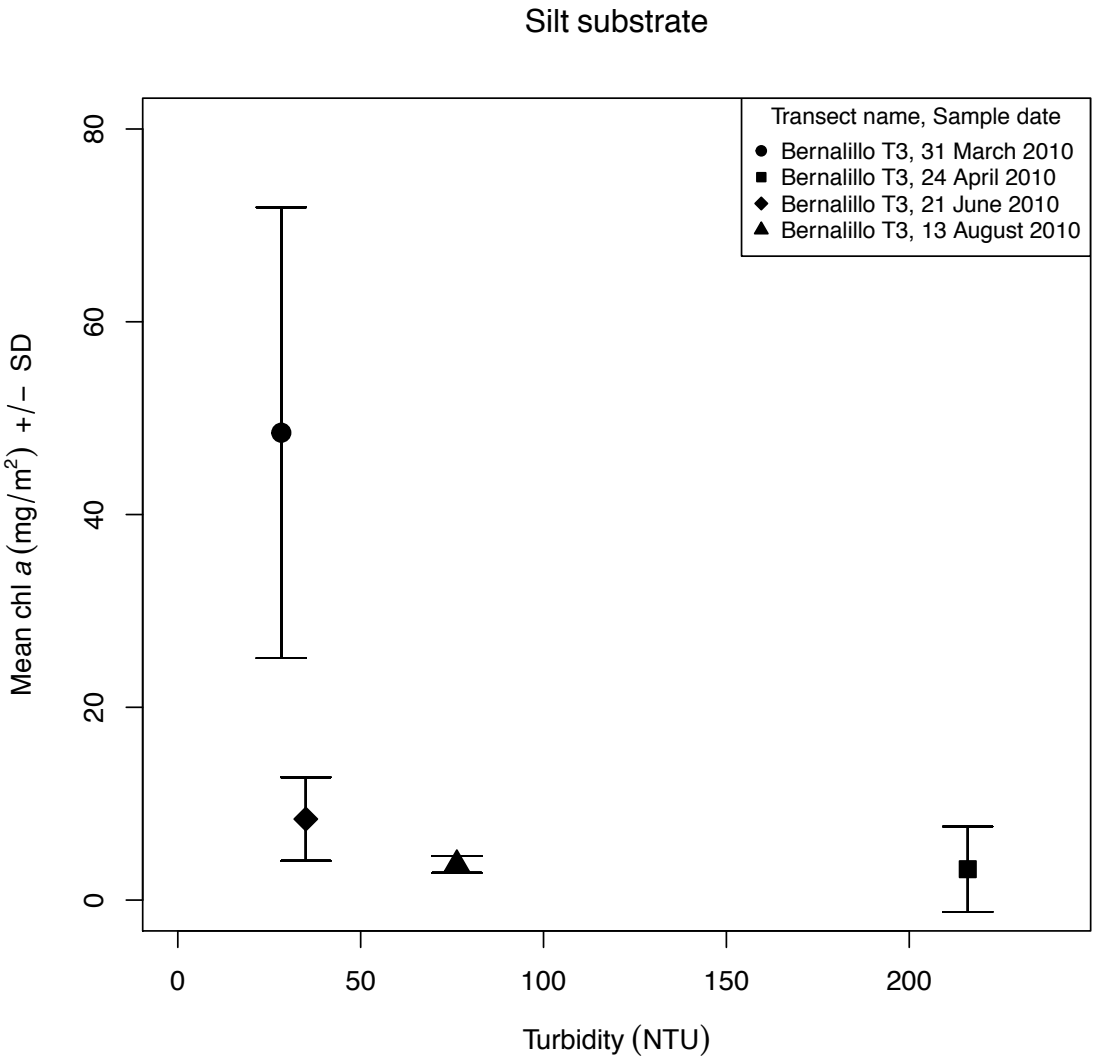

Figure 19: Scatter plot showing the relationship between turbidity and the concentration of chl *a* in the sand substrate samples with error bars showing one standard deviation about the mean.

3.1.3 Transect profiles

Figures 20, 21, and 22 show bed profiles for each transect with the associated measures of average velocity and chl *a* across each transect for each sampling date. These plots are organized by sampling location and sampling date and it is important to note that although the main channel at the Bernalillo site usually had a cobble substrate, flow conditions on 24 April 2010, forced the use of an alternate transect that happened to be sandy that day (possibly due to increased tributary inflow of fine sediments brought with flood pulses from spring snow melt). Sampling conditions (i.e., depth and velocity) did not always permit the collection of chl *a* samples at all the locations where depth was recorded resulting in gaps for some sampling dates. Positions with greater depth almost always have higher velocities and the almost mirrored transect profiles seen between the depth and average velocity plots show the strong relationship between position across the transect (i.e., distance and depth) and flow velocity.

As seen in the earlier plots, the sand transects show low concentrations of chl *a* in deeper and higher velocity areas of the transect, with the edges displaying the highest levels of chl *a*, possibly with the exception of the alternate main-channel transect Bernalillo T4 (Figure 20 and Figure 21). Again, the cobble and silt transects display somewhat different patterns, with relatively high concentrations of chl *a* seen in deep, high-velocity areas of the transects (Figures 21 and 22). Although the silt transects seem to show strong connections among chl *a*, depth, and velocity the highest levels of chl *a* are still generally seen in areas of reduced depth and velocity, but production is not limited to only those areas, as was seen in the sand transects. Of particular interest is the pattern seen in the 31 March 2010 profile in Figure 22 which shows a kind of bi-modal distribution of chl *a* across the transect. This may be due to the relatively stable submersion of areas farther away from the edge, avoiding desiccation, while still having more light and stable substrate not found in deeper, higher velocity areas of the transect.

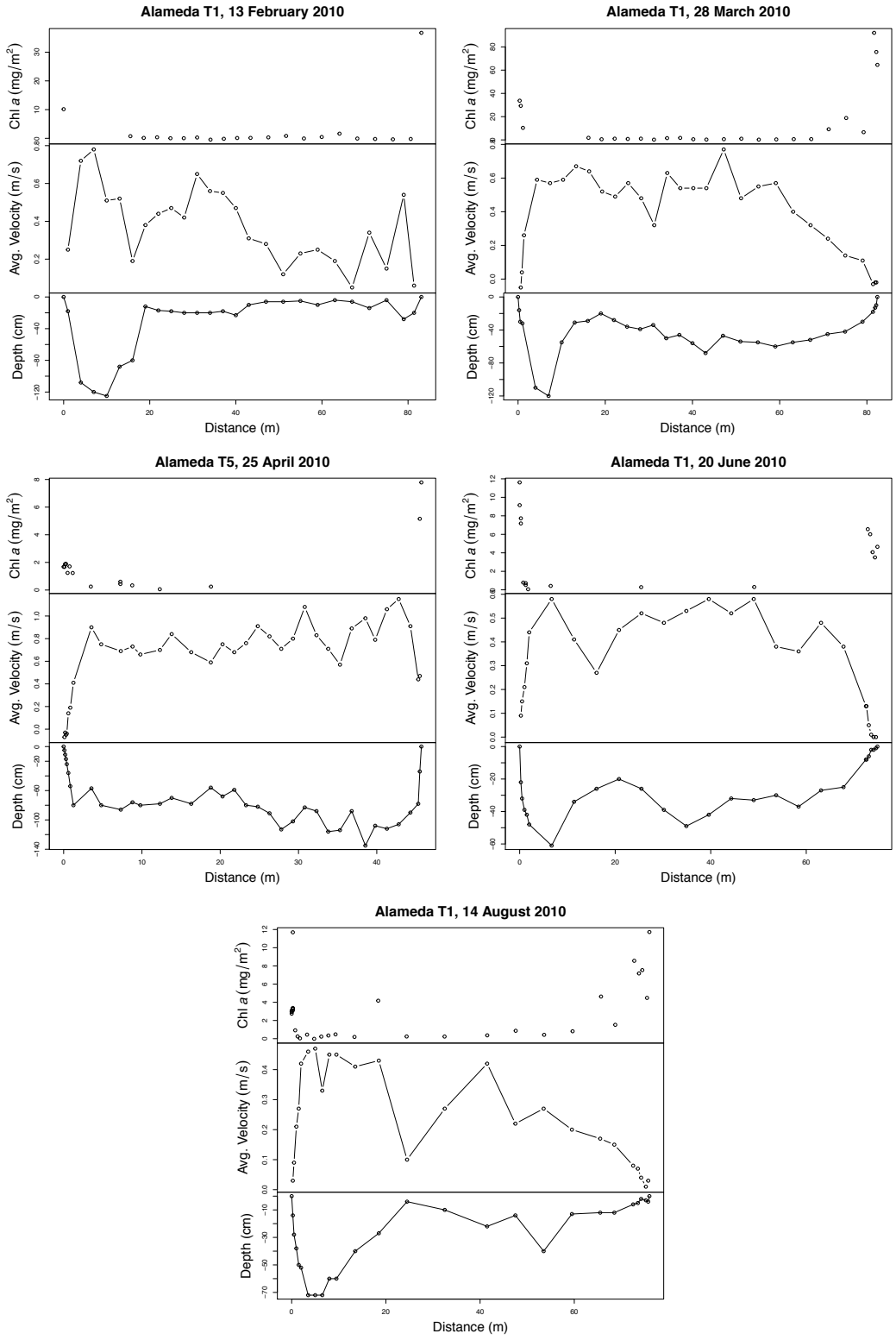

Figure 20: Depth and average velocity profiles with associated chl *a* measurements for the Alameda Blvd. main-channel transects T1 (sand) and the slightly down-stream alternate transect T5 (sand).

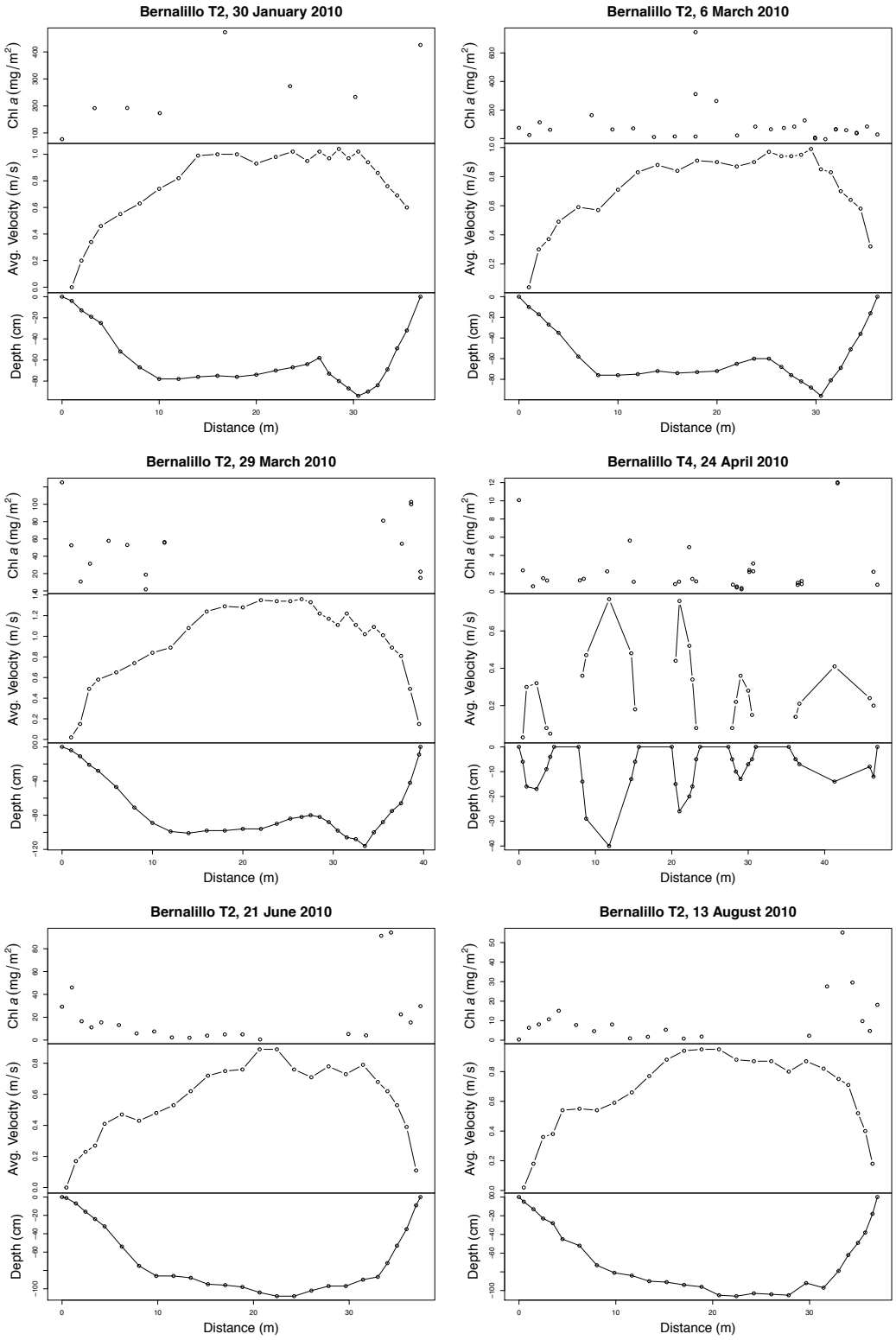

Figure 21: Depth and average velocity profiles with associated chl *a* measurements for the Bernalillo main-channel transects T2 (cobble substrate) and the alternate transect T4 (sand substrate).

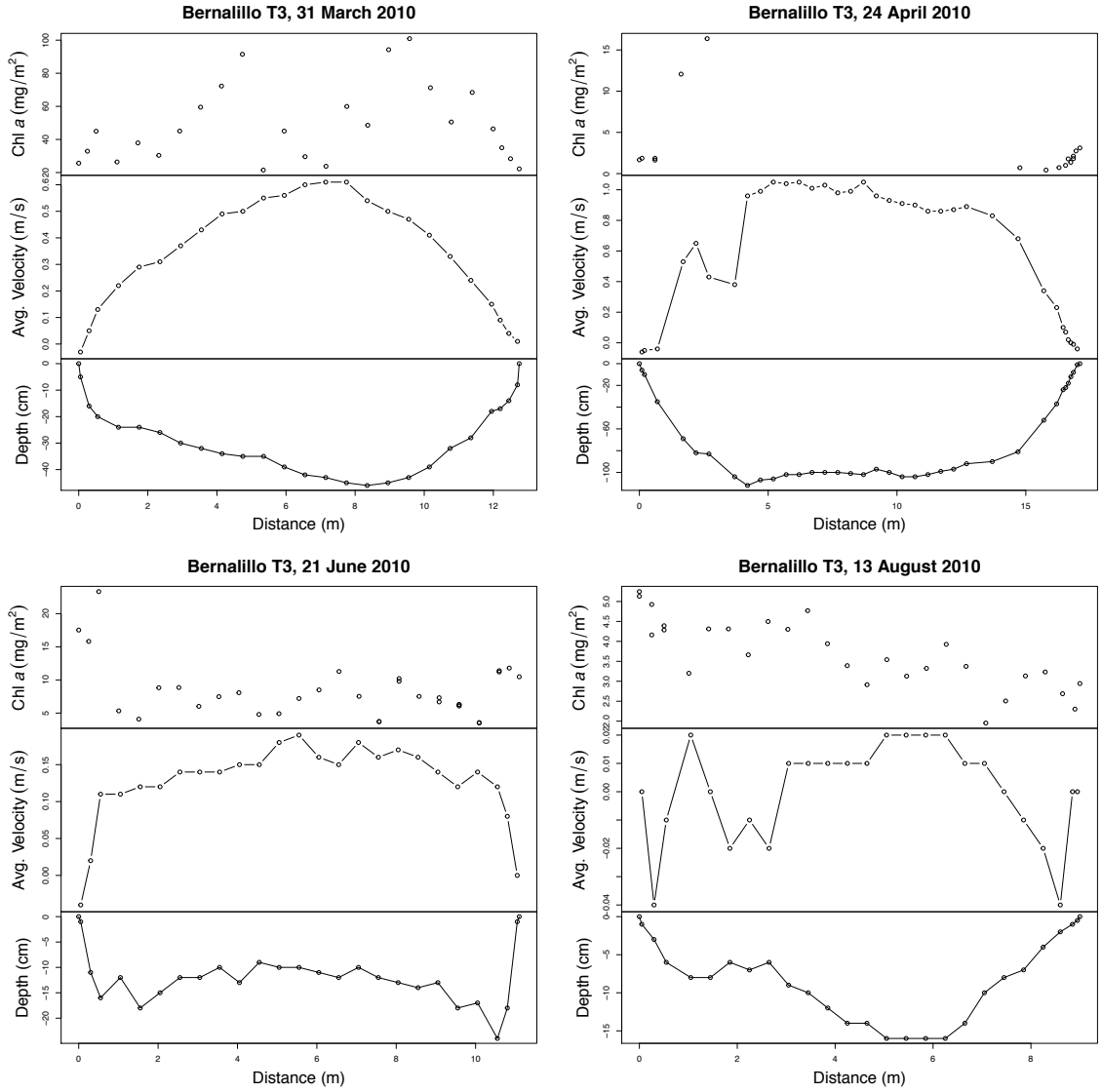

Figure 22: Depth and average velocity profiles with associated chl *a* measurements for the Bernalillo side-channel transect T3 (silt substrate).

3.2 Multivariate linear regression

In an effort to determine whether explanatory variables differed in their importance to the system, I developed a stepwise AIC method for variable selection and model validation. I began the variable selection with the following sets of variables: the data I recorded, log-transforms, and calculated data (i.e., discharge) as well as the irradiance data recorded by the NOAA ISIS station. These data provided an initial variable set of 113 variables. The final model selected using this method included 30 variables. The list of variables and associated linear-model coefficients found using this method is shown in Table 1. In order to investigate the importance of substrate, the data were divided into their respective substrate types and it should be noted that the variable names in 1 reflect their substrate type, but sand was used as the base case and it is not explicitly part of the variable name. Any variable that does not have "cobble" or "silt" in the name is associated with sand substrate data. The AIC rewards goodness of fit for each model as measured by residual error and penalizes the addition of predictors. This analysis provides insight into the important explanatory variables that when left out of the model decrease the goodness of fit. The remaining transformed variables suggest that those explanatory variables are more likely related to the response variable (chl a) by non-linear relationships.

Although the AIC is often used to reduce overfitting, it is still important to assess whether the model is being overfitted. Figure 23 shows a comparison between the model's predictive performance using training data that was used to select the model and test data that was left out to allow for the assessment of overfitting and model validation. I used mean absolute error (MAE) to compare the model fits, with an MAE for the test data that is 31.4% greater than that of the training data. It should be noted that the position in the list of coefficients and the magnitude of the coefficient value are not a score of the relative importance of the variable to the model.

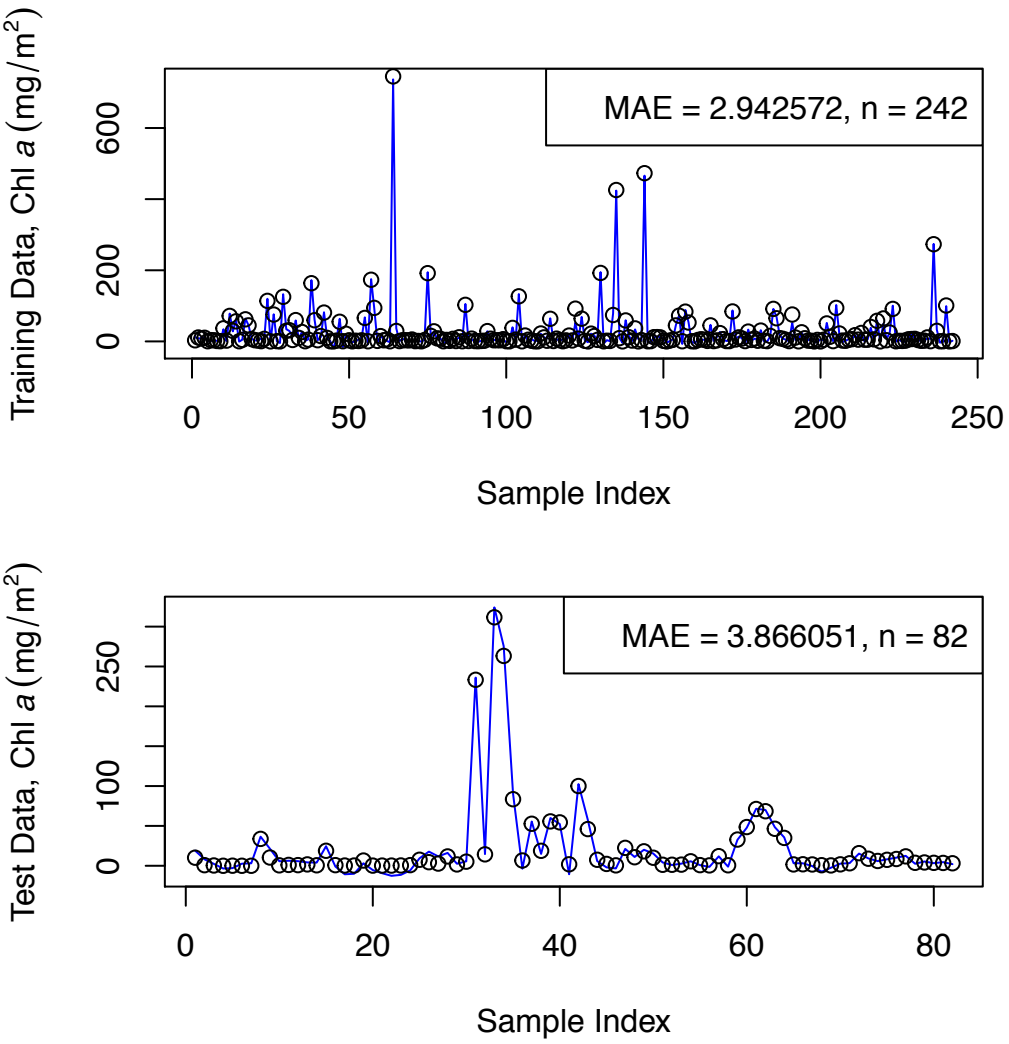

Figure 23: The model follows the basic linear multivariate form: $Y = (\beta_0 X_0) + (\beta_1 X_1) + \ldots + (\beta_n X_n)$ and this figure shows plots of the model predictions for chl *a* (blue line) as compared to my observations of chl *a* (black circles) after using stepwise AIC variable selection. The upper plot shows the model predictions for the data used to train the model and the lower plot shows the model predictions for test data not used during training. Mean absolute error (MAE) is used to compare the model fits. The MAE for the test data is 31.4% greater than the MAE for the training data.

	Variable Name	Coeffiecient Value
1	(Intercept)	269.06
2	SampleDate	-1.01
3	DistanceFromEdge.m	-0.36
4	RelativeDistanceFromEdge	8.57
5	Discharge.m.3_per_s	-0.55
6	Turbidity.NTU	0.54
7	Temperature.C	10.46
8	TDS.g_per_L	4667.05
9	Salinity	-2791.49
10	DO.mg_per_L	7.73
11	pH	-23.23
12	Pressure.mmHg	-1.31
13	irradiance.max	0.12
14	irradiance.mean	0.53
15	cobble	64.96
16	log.DistanceFromEdge.m	2.78
17	log.RelativeDistanceFromEdge	-3.32
18	log.Depth.cm	1.64
19	log.AverageVelocity.m_per_s	-8.90
20	sqrt.Chlorophyll_a.mg_per_m.2	3.64
21	sqrt.AverageVelocity.m_per_s	30.57
22	silt.Depth.cm	-0.16
23	silt.AverageVelocity.m_per_s	-26.98
24	silt.Chlorophyll_a.mg_per_m.2	0.76
25	silt.log.AverageVelocity.m_per_s	8.79
26	cobble.RelativeDistanceFromEdge	29.66
27	cobble.Depth.cm	0.17
28	cobble.AverageVelocity.m_per_s	-24.71
29	cobble.Chlorophyll_a.mg_per_m.2	0.87
30	cobble.log.Depth.cm	-11.29
31	cobble.log.AverageVelocity.m_per_s	11.07

Table 1: Values for the coefficients with their associated variable names remaining in the linear model after using a stepwise AIC model selection method. It should be noted that the position in the list of coefficients or the magnitude of the coefficient value are not scores of the relative importance of the variable to the model.

3.2.1 Photographs from field investigation

I took photographs of each transect during each sampling to document the sampling location, visually observable streamflow, weather conditions, and any other objects of interest. The following figures provide examples of note.

Figure 24: Main-channel sand transect at Alameda Blvd. Bridge, Alameda T1, 28 March 2010

Figure 25: Main-channel cobble transect at US Route 550 Bridge, Bernalillo T2, 29 March 2010

Figure 26: Side-channel silt transect near US Route 550 Bridge, Bernalillo T3, 31 March 2010

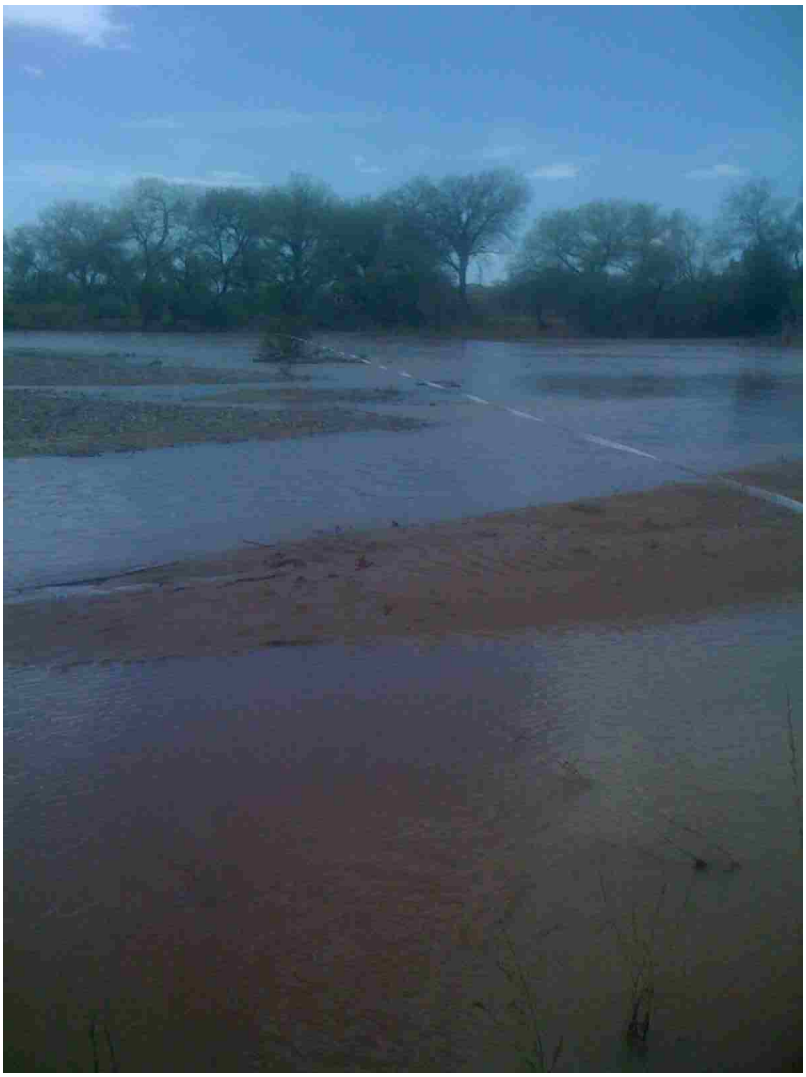

Figure 27: Alternate main-channel transect near US Route 550 Bridge, Bernalillo T4, 24 April 2010. Streamflow was too high in the usual Bernalillo T2 transect. Note the sandy substrate and the presence of several bar islands as opposed to the cobble substrate seen at all other sampling times.

Figure 28: Alternate main-channel transect near US Route 550 Bridge, Alameda T5, 25 April 2010. Note that the alternate transect is from the left edge of water to a vegetated island

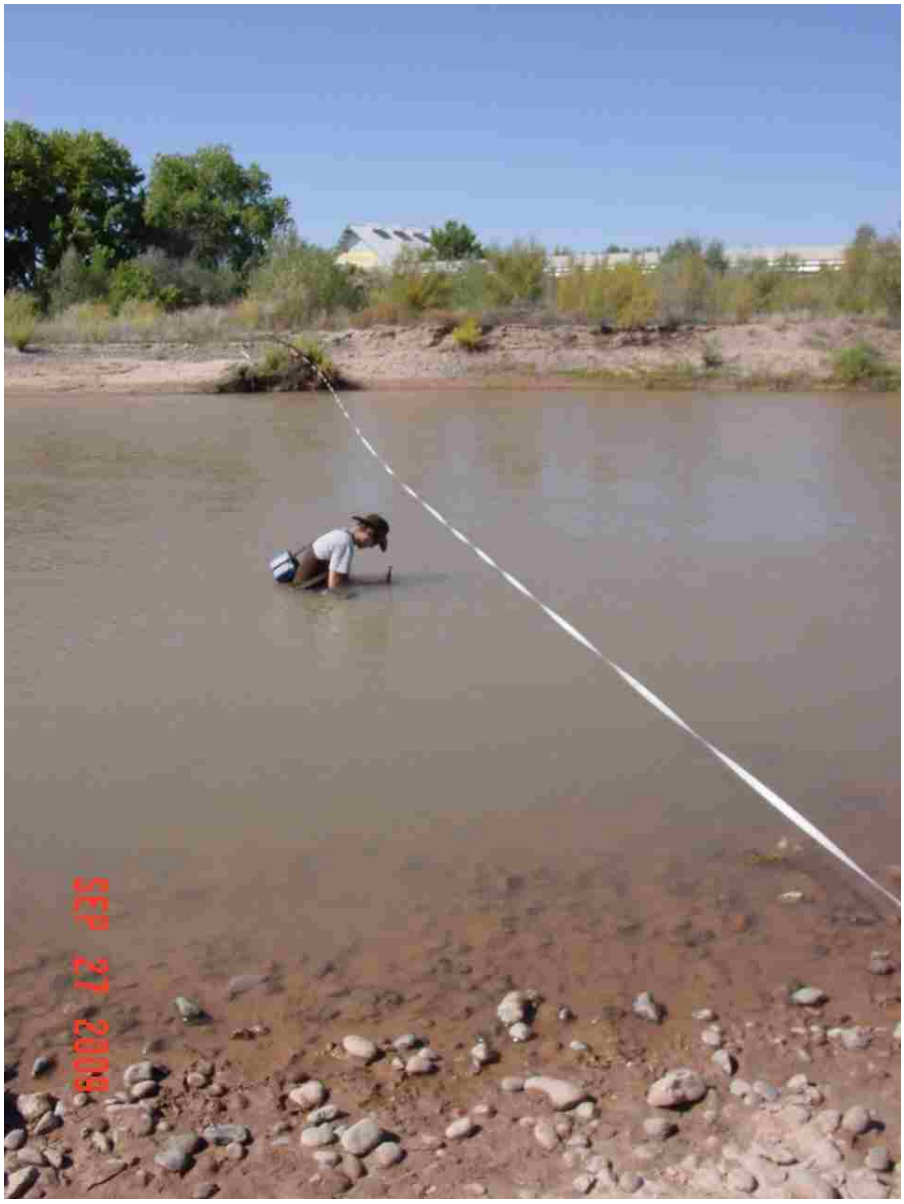

Figure 29: Sampling transect T2 across the Rio Grande main channel south of the US Route 550 Bridge in Bernalillo, New Mexico. (Photo taken by Stacy O. Scholle)

Figure 30: Example of extensive filamentous algal colonies on a cobble taken from the Bernalillo T2 sampling transect (shown in Figures 25 and 29) across the Rio Grande main channel south of the US Route 550 Bridge in Bernalillo, New Mexico. This cobble was found 18 m from the edge of the water at a depth of 76 cm.

Figure 31: Example of "bathtub-ring" instream primary productivity seen in the Rio Grande at the Sevilleta National Wildlife Refuge south of Albuquerque, New Mexico. (Photo taken by Corey A. Krabbenhoft)

4 Discussion

I initially hypothesized that edges would contain the highest levels of algal biomass because they are generally areas of reduced depth, lower flow velocity, and increased light availability, all of which tend to favor the attachment and growth of benthic algae (Bunn et al., 2003; Flynn et al., 2013). However, only the sand transects consistently show that relationship, as seen in the sand substrate plot in Figure 7. Although the low R^2 value does not suggest a linear relationship between distance from an edge and the amount of chlorophyll *a* sampled, there is still a clear negative relationship for the sand transects, in which distances relatively close to edges are shown to have the highest amounts of chl *a* and only minimal amounts at positions relatively distant from an edge. Figure 7 shows the all of the sand transect data together, but when the data are separated by transect and log-transformed, the linear models fit much better with R^2 values as high as 0.716 and clearly show the negative relationships between chl *a* and distance, depth, and velocity (Figures 8, 9, and 10). This pattern is seen in the transect profiles as well (Figure 20 and the Bernalillo T4 profile of Figure 21). The transect profiles show that flow velocity is closely and positively correlated with depth which likely plays a particularly important role for areas that have a sand substrate due to the relatively high bed mobility of sand. Especially as compared to the cobble or silt substrates, the sand transects almost exclusively display significant chl *a* concentrations in areas of the transect that have low flow velocities. Even in relatively shallow parts of the transects, chl *a* concentrations remain minimal until flow velocities are relatively low.

By comparison, the cobble and silt transects indicate that there is far more variability in the amount of chl *a* versus position, distance and depth, within the transect as compared to the sand transects, particularly in the aggregated data (Figure 7). Some of the fitted linear regression lines even suggest a positive relationship for some transects (Figures 7, 12, 16). The data shown in the silt plot of Figure 7, which

presents the distance from an edge versus chl *a* concentration for all of the silt substrate data, reveal that there are relationships between transect position and chl *a* that are distinctly different from those of the high-bed-load sand substrate.

The silt substrate channel, by virtue of lower flow velocity and fine sediment cohesion, is, at least transiently, an area of sediment deposition and very minimal scouring. This may help to explain why chl *a* concentrations can be higher than sand transects at farther relative distances from the edge. However, the highest levels of chl *a* are still not at the very edge of the water where flow velocity is lower and available light should be highest due to reduced depth. Perhaps lower velocity side channel flows provide a zone of maximal algal growth farther from the edge, and at higher depths, because of habitat disturbance at the distal edge (i.e., desiccation during low flows or scouring during higher flows). Zones of highest chl *a* concentrations may be close enough to the edge to receive enough light and avoid sediment disturbance but be far enough away from the edge to avoid drying due to fluctuations in water level. The Bernalillo T3, 31 March 2010 plot of Figure 22, particularly suggests this pattern.

The cobble substrate transect is an area of limited fine sediment supply in relation to transport capacity that results in an armored cobble riverbed. This makes the results I show in the cobble plot of Figure 7 particularly interesting; areas of high velocity flow and reduced light availability still provide high levels of chl *a* and support relatively large algal communities as seen in Figure 30. This may be do to the relative stability of the armored cobble substrate at this transect, which may provide a more stable habitat for the extensive filamentous algal growth seen there. Again, Figure 30 shows an example of the relatively large quantities of filamentous algae that can grow on the surface of cobbles at relatively large distances and greater depths in the cobble substrate transect and the turbidity plot in Figure 15 shows that the cobble transect has a smaller and lower range of turbidity measurements while having the

highest concentrations of chl *a*.

These results show that substrate appears to strongly influence the concentration of chl *a* measured in a given location within transects; relative distances at which no chl *a* was measured in the sand substrate yielded relatively high concentrations of chl *a* in both the silt and the cobble substrates (again see Figure 7). Also, these results generally support my initially hypothesized negative relationship between turbidity and the amount of chl *a*, as shown in the turbidity plot of Figure 4 and the cobble and silt transect turbidity plots (Figures 15 and 19). However, it should be noted that this pattern of decreasing chl *a* with increasing turbidity is not seen in the sand transects (Figure 11). This may be due to the relatively low concentrations of chl *a* measured anywhere outside of shallow edge habitats, which have more available light even during periods of high turbidity.

In this study I looked mostly at abiotic parameters that can affect the lateral distribution of benthic algae. However, there are likely many biotic factors, like differential grazing by fish and invertebrates, that may help to contribute to the differences in algal distributions seen in these data. Recent research suggests that *H. amarus* and other broadcast-spawning minnows have evolved life history characteristics that generally favor low flow velocity, fine sediment environments (Nicolas Medley and Shirey, 2013). Further, it has been suggested through gut-content studies that *H. amarus* preferentially feed on epipsammic diatoms (Magana, 2007; Cowley et al., 2006). It may be possible that high chl *a* values are seen in the Bernalillo data because grazing by minnows and other organisms is less prevalent in the Bernalillo main-channel transect due to the generally greater depth, higher flow velocities, cobble substrate, and filamentous (as opposed to diatomaceous) algal taxa present. Invertebrate grazers also probably have a great deal of influence on standing stocks of various algae types. Filamentous algae are probably most recalcitrant to grazing because of relatively high investment in structural components like holdfasts and other structures. High

velocity habitats may be least susceptible to grazing because of energetic demands of maintaining position in the water column, thus leading to high standing stocks of filamentous algae in high-velocity, deeper habitats. Conversely, epipsammic algae are higher quality and preferred among grazers. Stable isotope studies show that epipsammic algae are the predominant carbon source to higher trophic levels in the Rio Grande food web (Turner and Edwards, 2012). Grazers are concentrated around the edges, but growth rates may exceed consumption rates in these areas until later in the growing season (Pease et al., 2006).

Recent work has continued to develop the understanding of the connections among lateral variations in algal growth and various measures of abiotic environmental factors in lotic systems (Tonetto et al., 2014; Flynn et al., 2013). Tonetto et al. (2014) looks at the relationships between structural heterogeneity and the growth of benthic macroalgae. In their study they show that structural diversity in benthic surfaces (as studied on submerged tiles with various levels of surface complexity) can provide important refuges for algal attachment and growth. These refuges provide areas of reduced turbulence and sediment movement, potentially reducing the scouring of attached algae. Although their study was conducted in a tropical drainage basin (the Cervo River system in São Paulo State, south-eastern Brazil), the armored cobble bed of the Bernalillo 550 main-channel transect provides similar differences in benthic surface structure and may offer refuge for algal attachment and growth.

In the Flynn et al. (2013) study, an attempt is made to apply a mechanistic model to the lateral distribution of algae in the Yellowstone River in eastern Montana, USA. In their work these authors discuss the importance of many of the parameters I looked at in this study including the relationship among light and depth as well as velocity and scour. However, they found that it was difficult to effectively model the distribution of filamentous algae due to the differences in observed distribution of these species from other benthic algae in the system. They suggest, as I do here,

that complexities in substrate, among other fluvial geomorphic features, can strongly influence the lateral distribution of these species and that the differences among the habitat needs for these species can contribute to difficulties in the prediction of their distribution, warranting further investigation.

Further work may uncover relationships among abiotic factors and in-stream production that could be scaled to include reach-length estimates of production in this and similar systems, as approximated in the Flynn et al. (2013) study for the Yellowstone River. However, as discussed, these systems can be difficult to model due to complex, often counter intuitive interactions of fluvial geomorphic forms and processes that may facilitate the growth of filamentous algae in deep, high-flow regions of the bed-profile far from edges. In this study I have recorded this pattern within the middle Rio Grande. However, I have found that at least in sandy-bottom reaches of the system, edges can be critical zones of benthic algal growth. These seemingly opposing patterns suggest that there are deeper relationships linking mechanisms of fluvial geomorphic forms and instream productivity. This study illuminates the surface of some of these relationships with Figure 23 and Table 1 providing a study of the important variables suggested by our data and providing a compelling multivariate linear relationship among them. This work highlights the important interface between fluvial geomorphology and aquatic ecology and contributes to the growing body of knowledge surrounding this system.

References

Benda, L., N. Poff, D. Miller, T. Dunne, G. Reeves, G. Pess, and M. Pollock
2004. The network dynamics hypothesis: how channel networks structure riverine habitats. *BioScience*, 54(5):413–427. 1

Biggs, B. J. F., R. A. Smith, and M. J. Duncan
1999. Velocity and sediment disturbance of periphyton in headwater streams: Biomass and metabolism. *Journal of the North American Benthological Society*, 18(2):pp. 222–241. 8

Bunn, S. and P. Davies
1999. Aquatic food webs in turbid, arid-zone rivers: preliminary data from Cooper Creek, western Queensland. In *A Freeflowing River: the Ecology of the Paroo River*, R. Kingsford, ed., Pp. 67–76. Sydney: New South Wales Parks and Wildlife Service. 1

Bunn, S., P. Davies, and M. Winning
2003. Sources of organic carbon supporting the food web of an arid zone floodplain river. *Freshwater Biology*, 48(4):619–635. 1, 47

Carignan, R., D. Planas, and C. Vis
2000. Planktonic production and respiration in oligotrophic shield lakes. *Limnology and Oceanography*, 45(1):189–199. 8

Cavanaugh, J. E.
2007. *Akaike Information Criterion*, Pp. 16–18. SAGE Publications, Inc., 0 edition. 10

Cowley, D. E., P. D. Shirey, and M. D. Hatch
2006. Ecology of the rio grande silvery minnow (cyprinidae: Hybognathus amarus) inferred from specimens collected in 1874. *Reviews in Fisheries Science*, 14(1):111–125. 49

Dahl, D. B.
2014. *xtable: Export tables to LaTeX or HTML*. R package version 1.7-4. 9

Fisher, S. G., J. B. Heffernan, R. A. Sponseller, and J. R. Welter
2007. Functional ecomorphology: Feedbacks between form and function in fluvial landscape ecosystems. *Geomorphology*, 89(1–2):84 – 96. 36th Binghamton Geomorphology Symposium Geomorphology and Ecosystems. 2

Flynn, K. F., S. C. Chapra, and M. W. Suplee
2013. Modeling the lateral variation of bottom-attached algae in rivers. *Ecological Modelling*, 267(0):11 – 25. 1, 47, 50, 51

Hall, R. O., J. L. Tank, D. J. Sobota, P. J. Mulholland, J. M. O'Brien, W. K. Dodds, J. R. Webster, H. M. Valett, G. C. Poole, B. J. Peterson, J. L. Meyer,

W. H. McDowell, S. L. Johnson, S. K. Hamilton, N. B. Grimm, S. V. Gregory, C. N. Dahm, L. W. Cooper, L. R. Ashkenas, S. M. Thomas, R. W. Sheibley, J. D. Potter, B. R. Niederlehner, L. T. Johnson, A. M. Helton, C. M. Crenshaw, A. J. Burgin, M. J. Bernot, J. J. Beaulieu, and C. P. Arangob
2009. Nitrate removal in stream ecosystems measured by 15n addition experiments: Total uptake. *Limnology and Oceanography*, 54(3):653–665. 3

Hamilton, S., J. Tank, D. Raikow, E. Siler, N. Dorn, and N. Leonard
2004. The role of instream vs allochthonous N in stream food webs: modeling the results of an isotope addition experiment. *Journal of the North American Benthological Society*, 23(3):429–448. 1

Hicks, B., J. DeLuisi, and D. Matt
1996. The noaa integrated surface irradiance study (isis)-a new surface radiation monitoring program. *Bulletin Of The American Meteorological Society*, 77(12):2857–2864. 9

Junk, W., P. Bayley, R. Sparks, et al.
1989. The flood pulse concept in river-floodplain systems. *Canadian Special Publication of Fisheries and Aquatic Sciences*, 106:110–127. 2

Loeb, S.
1981. An in situ method for measuring the primary productivity and standing crop of the epilithic periphyton community in lentic systems. *Limnology and oceanography*, 26(2):394–399. 8

Lorenzen, C. J.
1967. Determination of chlorophyll and pheo-pigments: Spectrophotometric equations1. *Limnology and Oceanography*, 12(2):343–346. 9

Magana, H. A.
2007. *A case for classifying the Rio Grande silvery minnow (Hybognathus amarus) as an omnivore*. PhD thesis. Copyright - Copyright ProQuest, UMI Dissertations Publishing 2007; Last updated - 2015-08-26; First page - n/a. 49

Micheli, E. and J. Kirchner
2002. Effects of wet meadow riparian vegetation on streambank erosion. 2. Measurements of vegetated bank strength and consequences for failure mechanics. *Earth Surface Processes and Landforms*, 27(7):687–697. 2

Newbold, J., P. Mulholland, J. Elwood, and R. O'Neill
1982a. Organic carbon spiralling in stream ecosystems. *Oikos*, 38(3):266–272. 2

Newbold, J., R. O'Neill, J. Elwood, and W. Van Winkle
1982b. Nutrient spiralling in streams: implications for nutrient limitation and invertebrate activity. *The American Naturalist*, 120(5):628–652. 2

Nicolas Medley, C. and P. D. Shirey
2013. Review and reinterpretation of rio grande silvery minnow reproductive ecology using egg biology, life history, hydrology, and geomorphology information. *Ecohydrology*, 6(3):491–505. 49

Ortiz, R. M.
2004. A river in transition: geomorphic and bed sediment response to cochiti dam on the middle rio grande, bernalillo to albuquerque, new mexico. Master's thesis, The University of New Mexico. 3, 5

Pease, A., J. Davis, M. Edwards, and T. Turner
2006. Habitat and resource use by larval and juvenile fishes in an arid-land river (Rio Grande, New Mexico). *Freshwater Biology*, 51(3):475–486. 1, 50

Poff, N. and J. Ward
1990. Physical habitat template of lotic systems: Recovery in the context of historical pattern of spatiotemporal heterogeneity. *Environmental Management*, 14(5):629–645. 7

Potapova, M. G. and D. F. Charles
2002. Benthic diatoms in usa rivers: distributions along spatial and environmental gradients. *Journal of Biogeography*, 29(2):167–187. 6

R Core Team
2015. *R: A Language and Environment for Statistical Computing*. R Foundation for Statistical Computing, Vienna, Austria. 9

Rantz, S.
1982. Measurement and computation of streamflow: Volume 1. Measurement of stage and discharge. Volume 2. Computation of discharge. *USGS Water-Supply Paper 2175*, P. 631. 6, 7

Renschler, C., M. Doyle, and M. Thoms
2007. Geomorphology and ecosystems: challenges and keys for success in bridging disciplines. *Geomorphology*, 89(1-2):1–8. 2

Sarkar, D.
2008. *Lattice: Multivariate Data Visualization with R*. New York: Springer. ISBN 978-0-387-75968-5. 9

Sartory, D. and J. Grobbelaar
1984. Extraction of chlorophyll a from freshwater phytoplankton for spectrophotometric analysis. *Hydrobiologia*, 114(3):177–187. 8

Swanson, B. J., G. A. Meyer, and J. E. Coonrod
2011. Historical channel narrowing along the rio grande near albuquerque, new mexico in response to peak discharge reductions and engineering: magnitude and uncertainty of change from air photo measurements. *Earth Surface Processes and Landforms*, 36(7):885–900. 1, 3

Swanson, F., T. Kratz, N. Caine, and R. Woodmansee
1988. Landform effects on ecosystem patterns and processes. *BioScience*, 38(2):92–98. 1

Thoms, M. C. and M. Parsons
2002. Eco-geomorphology: an interdisciplinary approach to river science. *International Association of Hydrological Sciences, Publication*, (276):113–119. 2

Tonetto, A. F., R. Cardoso-Leite, C. K. Peres, P. d. C. Bispo, and C. C. Z. Branco
2014. The effects of habitat complexity and hydraulic conditions on the establishment of benthic stream macroalgae. *Freshwater Biology*, 59(8):1687–1694. 50

Turner, T. F. and M. S. Edwards
2012. Aquatic foodweb structure of the rio grande assessed with stable isotopes. *Freshwater Science*, 31(3):pp. 825–834. 50

Turnipseed, D. P. and V. B. Sauer
2010. Discharge measurements at gaging stations. Technical report, US Geological Survey. 6

Van Dam, H., A. Mertens, and J. Sinkeldam
1994. A coded checklist and ecological indicator values of freshwater diatoms from the netherlands. *Netherland Journal of Aquatic Ecology*, 28(1):117–133. 6

Van Horn, D., L. Zeglin, and C. Dahm
2006. Seasonal and longitudinal trends in the middle rio grande water quality. *Bulletin of the North American Benthological Society*, 23:351. 3

Xie, Y.
2014. knitr: A comprehensive tool for reproducible research in R. In *Implementing Reproducible Computational Research*, V. Stodden, F. Leisch, and R. D. Peng, eds. Chapman and Hall/CRC. ISBN 978-1466561595. 9

Xie, Y.
2015a. *Dynamic Documents with R and knitr*, 2nd edition. Boca Raton, Florida: Chapman and Hall/CRC. ISBN 978-1498716963. 9

Xie, Y.
2015b. *knitr: A General-Purpose Package for Dynamic Report Generation in R*. R package version 1.11. 9